SWAN

TECHNICAL DOCUMENTATION

SWAN Cycle III version 40.51

SWAN TECHNICAL DOCUMENTATION

by	:	The SWAN team
mail address	:	Delft University of Technology Faculty of Civil Engineering and Geosciences Environmental Fluid Mechanics Section P.O. Box 5048 2600 GA Delft The Netherlands
e-mail	:	swan-info-citg@tudelft.nl
home page	:	*http://www.fluidmechanics.tudelft.nl/swan/index.htm*http://www.fluidmec

Contents

Chapter 1

Introduction

The main goal of the SWAN model is to solve the spectral action balance equation without any *a priori* restrictions on the spectrum for the evolution of wave growth. This equation represents the effects of spatial propagation, refraction, shoaling, generation, dissipation and nonlinear wave-wave interactions. The basic scientific philosophy of SWAN is identical to that of WAM cycle 3. SWAN is a third-generation wave model and it uses the same formulations for the source terms.

Whereas the WAM model considers problems on oceanic scales, with SWAN wave propagation is calculated from deep water to the surf zone. Since, WAM makes use of explicit propagation schemes in geographical and spectral spaces, it requires very small grid sizes in shallow water and is thus unsuitable for applications to coastal regions. For that reason, SWAN employs implicit schemes, which are more robust and economic in shallow water than the explicit ones. Note that SWAN may be less efficient on oceanic scales than WAM.

1.1 Historical background

Over the past two decades, a number of advanced spectral wind-wave models, known as third-generation models, has been developed such as WAM (WAMDI Group, 1988), WAVEWATCH III (Tolman, 1991), TOMAWAC (Benoit *et al.*, 1996) and SWAN (Booij *et al.*, 1999). These models solve the spectral action balance equation without any *a priori* restrictions on the spectrum for the evolution of wave growth.

Based on the wave action balance equation with sources and sinks, the shallow water wave model SWAN (acronym for Simulating WAves Nearshore) is an extension of the deep water third-generation wave models. It incorporates the state-of-the-art formulations for the deep water processes of wave generation, dissipation and the quadruplet wave-wave interactions from the WAM model (Komen *et al.*, 1994). In shallow water, these processes have been supplemented with the state-of-the-art formulations for dissipation due to bottom friction, triad wave-wave interactions and depth-induced breaking. SWAN is fully spectral (in all directions and frequencies) and computes the evolution of wind waves in coastal regions with shallow water and ambient current.

SWAN is developed at Delft University of Technology and is freely available from
*http://www.fluidmechanics.tudelft.nl/swan/index.htm*http://www.fluidmechanics.tudelft.nl/sw
It is used by many goverment authorities, research institutes and consultants worldwide. The feedback has widely indicated the reliability of SWAN in different experiment and field cases.

Initially, the SWAN cycle 1 was formulated to be able to handle only stationary conditions on a rectangular grid. Later on, SWAN cycle 2 model has been developed. This is considered as the second step in the development of SWAN models. Cycle 2 of SWAN is stationary and optionally non-stationary. It can compute the wave propagation not only on a regular rectangular grid, but also on a curvilinear grid. Previous official versions 30.62, 30.75, 40.01 and 32.10 belong to the cycle 2 of SWAN.

This section is under preparation.

1.2 Purpose and motivation

The purpose of this document is to provide relevant information on the mathematical models and numerical techniques for the simulation of spectra of random short-crested, wind-generated waves in coastal regions. Furthermore, this document explains the essential steps involved in the implementation of various numerical methods, and thus provides an adequate reference with respect to the structure of the SWAN program.

1.3 Readership

This document is, in the first place, addressed to those, who wish to modify and to extend mathematical and numerical models for shallow wind-wave problems. However, this material is also useful for those who are interested in the application of the techniques discussed here. The text assumes the reader has basic knowledge of analysis, partial differential equations and numerical mathematics and provides what is needed both in the main text and in the appendices.

1.4 Scope of this document

SWAN is a third-generation wave model for obtaining realistic estimates of wave parameters in coastal areas, lakes and estuaries from given wind, bottom and current conditions. However, SWAN can be used on any scale relevant for wind-generated surface gravity waves. The model is based on the wave action balance equation (or energy balance in the absence of currents) with sources and sinks. Good introductory texts on the background of SWAN are Young (1999) and Booij *et al.* (1999).

The following wave propagation processes are represented in SWAN:

- propagation through geographic space,
- refraction due to spatial variations in bottom and current,
- diffraction,
- shoaling due to spatial variations in bottom and current,
- blocking and reflections by opposing currents and
- transmission through, blockage by or reflection against obstacles.

The following wave generation and dissipation processes are represented in SWAN:

- generation by wind,
- dissipation by whitecapping,

- dissipation by depth-induced wave breaking,
- dissipation by bottom friction and
- wave-wave interactions in both deep and shallow water.

In addition, the wave-induced set-up of the mean sea surface can be computed in SWAN. However, wave-induced currents are not computed by SWAN. In 1D cases, computation of wave-induced set-up is based on exact shallow water equations, whereas in 2D cases they need to be approximated since the effects of wave-induced currents are ignored.

Diffraction is modelled in a restrict sense, so the model should be used in areas where variations in wave height are large within a horizontal scale of a few wave lengths. However, the computation of diffraction in arbitrary geophysical conditions is rather complicated and requires considerable computing effort. To avoid this, a phase-decoupled approach, as described in (Holthuijsen *et al.*, 2003), is employed so that same qualitative behaviour of spatial redistribution and changes in wave direction is obtained.

SWAN is stationary and optionally non-stationary and can be applied in Cartesian or curvi-linear (recommended only for small scales) or spherical (small scales and large scales) co-ordinates. The stationary mode should be used only for waves with a relatively short residence time in the computational area under consideration, i.e. the travel time of the waves through the region should be small compared to the time scale of the geophysical conditions (wave boundary conditions, wind, tides and storm surge).

1.5 Overview

The remainder of this document is subdivided as follows: In Chapter 2 the action balance equations used in SWAN are presented. Next, each source term of the governing equations is in depth described. In Chapter 3 the main characteristics of the finite difference method for the discretization of the governing equations in irregular horizontal planes are outlined. Various differencing schemes for spatial propagation are reported. Chapter 4 is concerned with discussing several boundary conditions and their implementation. Chapter 5 is devoted to the design of the two-dimensional wave set-up of sea surface. Chapter 6 is devoted to the linear solvers for the solution of

the resulted linear systems of equations. Chapter 7 deals with some consideration on parallelization of SWAN on distributed memory architectures. Chapter 8 concludes this document by summarizing the overall solution algorithm of SWAN.

This document, however, is not intended as being complete. Although, this document describes the essential steps involved in the simulation of wind-generated waves, so that the user can see which can be modified or extended to solve a particular problem properly, some issues involved in SWAN are not included. Below, a list of these issues is given, of which the information maybe available elsewhere:

- RIAM,
- reflections, and
- diffraction.

1.6 Acknowledgements

The present SWAN team are grateful to the contributors from the very first days of SWAN which took place at the Delft University of Technology in Delft, The Netherlands in 1993: Nico Booij and Leo Holthuijsen.

We further want to acknowledge all contributors who helped us to improve SWAN, reported bugs, and tested SWAN thoroughly: Tim Campbell, John Cazes, IJsbrand Haagsma, Annette Kieftenburg, Ekaterini Kriezi, Roberto Padilla-Hernandez, Roeland Ris, Erick Rogers, Andre van der Westhuijsen and Marcel Zijlema.

Many thanks are due to Gerbrant van Vledder and Noriaki Hashimoto who provided the source code for exact computation of four wave-wave interations, XNL and RIAM, respectively.

It was also the important role which SWAN played in several projects, mostly funded by the Office of Naval Research (USA), which helped a lot to develop and maintain SWAN. The present version of SWAN is supported by Rijkswaterstaat (as part of the Ministry of Transport, Public Works and Water Management, The Netherlands).

We are finally grateful to all those other people working on the Public Domain Software without which a project like SWAN would be unthinkable: Linux, Intel, GNU F95, LaTeX, MPICH and many others.

Chapter 2

Governing equations

2.1 Spectral description of wind waves

Wind generated waves have irregular wave heights and periods, caused by the irregular nature of wind. Due to this irregular nature, the sea surface is continually varying, which means that a deterministic approach to describe the sea surface is not feasible. On the other hand, statistical properties of the surface, like average wave height, wave periods and directions, appear to vary slowly in time and space, compared to typical wave periods and wave lengths. The surface elevation of waves in the ocean, at any location and any time, can be seen as the sum of a large number of harmonic waves, each of which has been generated by turbulent wind in different places and times. They are therefore statistically independent in their origin. According to linear wave theory, they remain independent during their journey across the ocean. Under these conditions, the sea surface elevation on a time scale of one hundred characterstic wave periods is sufficiently well described as a stationary, Gaussian process. The sea surface elevation in one point as a function of time can be described as

$$\eta(t) = \sum_i a_i \cos(\sigma_i t + \alpha_i) \tag{2.1}$$

with η the sea surface elevation, a_i the amplitude of the i^{th} wave component, σ_i the relative radian or circular frequency of the i^{th} wave component in the presence of the ambient current (equals the absolute radian frequency ω when no ambient current is present) and α_i the random phase of the i^{th} wave component. This is called the random-phase model.

In the presene of the ambient current, it is assumed that it is uniform with respect to the vertical co-ordinate and the changes in the mean flow within a wave length are so small that they affect only negligibly the dispersion relation. The absolute radian frequency ω then equals the sum of the relative radian frequency σ and the multiplication of the wave number and ambient current velocity vectors:

$$\omega = \sigma + \vec{k} \cdot \vec{u} \tag{2.2}$$

which is the usual Doppler shift. For linear waves, the relative frequency is given by

$$\sigma^2 = gk \tanh(kd) \tag{2.3}$$

where g is the acceleration of gravity and d is the water depth.

Ocean waves are chaotic and a description in the time domain is rather limited. Alternatively, many manipulations are more readily described and understood with the variance density spectrum, which is the Fourier transform of the auto-covariance function of the sea surface elevation:

$$E'(f) = \int_{-\infty}^{+\infty} C(\tau) e^{-2\pi i f \tau} d\tau \tag{2.4}$$

with

$$C(\tau) = < \eta(t)\eta(t+\tau) > \tag{2.5}$$

where $C(\tau)$ is auto-covariance function, $<>$ represents mathematical expectation of random variable and $\eta(t)$, $\eta(t+\tau)$ represent two random processes of sea surface elevation, τ represents the time lag.

In the field of ocean wave theory it is conventional to degfine a spectrum $E(f)$ slightly different from the above one:

$$E(f) = 2E'(f) \quad \text{for } f \geq 0 \quad \text{and } E(f) = 0 \quad \text{for } f < 0 \tag{2.6}$$

The description of water waves through the defined variance density spectrum $E(f)$ is called spectral description of water waves. It can be proved that the variance of the sea surface elevation is given by

$$< \eta^2 > = C(0) = \int_0^{+\infty} E(f) df \tag{2.7}$$

which indicates that the spectrum distributes the variance over frequencies. $E(f)$ should therefore be interpreted as a variance density. The dimensions

of $E(f)$ are m^2/Hz if the elevation is given in m and the frequencies in Hz.

The variance $< \eta^2 >$ is equal to the total energy E_{tot} of the waves per unit surface area if multiplied with a properly chosen coefficient:

$$E_{\text{tot}} = \frac{1}{2}\rho_w g < \eta^2 > \tag{2.8}$$

The terms *variance density spectrum* and energy density spectrum will therefore be used indiscriminately in this document.

In many wave problems it is not sufficient to define the energy density as a function of frequency alone. It is mostly required to distribute the wave energy over directions as well. This spectrum, which distributes the wave energy over frequencies and directions, will be denoted with $E(f, \theta)$. As the total energy density at a frequency f is dstributed over the directions θ in $E(f, \theta)$, it follows that:

$$E(f) = \int_0^{2\pi} E(f, \theta) d\theta \tag{2.9}$$

The energy density spectrum $E(f)$ and $E(f, \theta)$ are depicted in Figure 2.1. Based on the energy density spectrum, the integral wave parameters can be obtained. These parameters can be expressed in terms of the so-called $n-$th moment of the energy density spectrum:

$$m_n = \int_0^{\infty} f^n E(f) df \tag{2.10}$$

So, the variance of the sea surface elevation is given by $m_0 =< \eta^2 >$. Well-known parameters are the significant wave height:

$$H_s = 4\sqrt{m_0} \tag{2.11}$$

and some wave periods:

$$T_{m01} = \frac{m_0}{m_1}, \quad T_{m02} = \sqrt{\frac{m_0}{m_2}}, \quad T_{m-10} = \frac{m_{-1}}{m_0} \tag{2.12}$$

In SWAN, the energy density spectrum $E(\sigma, \theta)$ is generally used. On a larger scale the spectral energy density function $E(\sigma, \theta)$ becomes a function of space and time and wave dynamics should be considered to determine the evolution of the spectrum in space and time. For brevity, the notation $E(\sigma, \theta)$ will still be used.

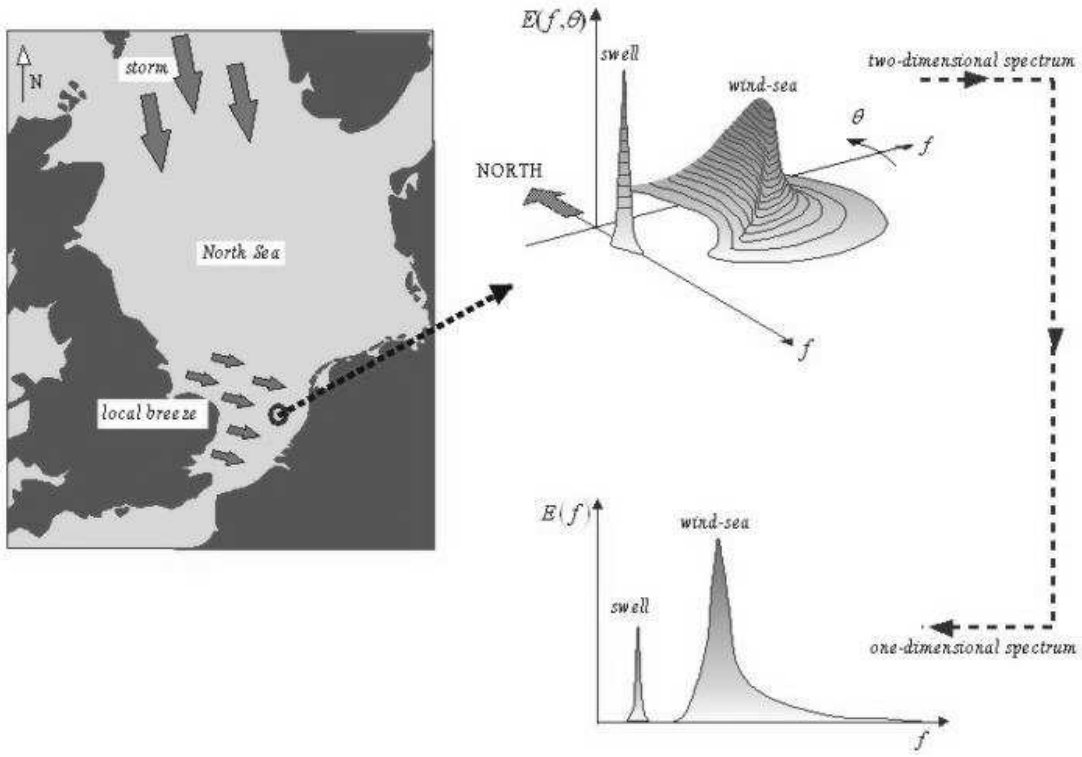

Figure 2.1: Illustrations of 1D and 2D wave spectra. (Reproduced from Holthuijsen (2005) with permission of Cambridge University Press.)

2.2 Propagation of wave energy

2.2.1 Wave kinematics

Using the linear wave theory and the conversion of wave crests, the wave propagation velocities in spatial space and spectral space can be obtained from the kinematics of a wave train (Whitham, 1974; Mei, 1983):

$$\frac{d\vec{x}}{dt} = (c_x, c_y) = \vec{c_g} + \vec{u} = \frac{1}{2}\left(1 + \frac{2kd}{\sinh(2kd)}\right)\frac{\sigma\vec{k}}{k^2} + \vec{u} \qquad (2.13)$$

$$\frac{d\sigma}{dt} = c_\sigma = \frac{\partial\sigma}{\partial d}\left(\frac{\partial d}{\partial t} + \vec{u}\cdot\nabla_{\vec{x}}d\right) - c_g\vec{k}\cdot\frac{\partial\vec{u}}{\partial s}$$

$$\frac{d\theta}{dt} = c_\theta = -\frac{1}{k}\left(\frac{\partial\sigma}{\partial d}\frac{\partial d}{\partial m} + \vec{k}\cdot\frac{\partial\vec{u}}{\partial m}\right)$$

where c_x, c_y are the propagation velocities of wave energy in spatial $x-$, $y-$space, c_σ and c_θ are the propagation velocities in spectral space $\sigma-$, $\theta-$space, d is water depth, s is the space co-ordinate in the wave propagation direction of θ and m is a co-ordinate perpendicular to s. Furthermore,

$$\vec{k} = (k_x, k_y), \quad \vec{u} = (u_x, u_y) \tag{2.14}$$

In addition, the operator d/dt denotes the total derivative along a spatial path of energy propagation, and is defined as

$$\frac{d}{dt} = \frac{\partial}{\partial t} + (\vec{c_g} + \vec{u}) \cdot \nabla_{\vec{x}} \tag{2.15}$$

2.2.2 Spectral action balance equation

All information about the sea surface is contained in the wave variance spectrum or energy density $E(\sigma, \theta)$, distributing wave energy over (radian) frequencies σ (as observed in a frame of reference moving with current velocity) and propagation directions θ (the direction normal to the wave crest of each spectral component). Usually, wave models determine the evolution of the action density $N(\vec{x}, t; \sigma, \theta)$ in space $\vec{x}$ and time t. The action density is defined as $N = E/\sigma$ and is conserved during propagation in the presence of ambient current, whereas energy density E is not (Whitman, 1974). It is assumed that the ambient current is uniform with respect to the vertical co-ordinate and is denoted as $\vec{U}$.

The evolution of the action density N is governed by the action balance equation, which reads (e.g., Mei, 1983; Komen *et al.*, 1994):

$$\frac{\partial N}{\partial t} + \nabla_{\vec{x}} \cdot [(\vec{c}_g + \vec{U})N] + \frac{\partial c_\sigma N}{\partial \sigma} + \frac{\partial c_\theta N}{\partial \theta} = \frac{S_{\text{tot}}}{\sigma} \tag{2.16}$$

The left-hand side is the kinematic part of this equation. The second term denotes the propagation of wave energy in two-dimensional geographical $\vec{x}$-space, with the group velocity $\vec{c}_g = \partial\sigma/\partial\vec{k}$ following from the dispersion relation $\sigma^2 = g|\vec{k}| \tanh(|\vec{k}|d)$ where $\vec{k}$ is the wave number vector and d the water depth. The third term represents the effect of shifting of the radian frequency due to variations in depth and mean currents. The fourth term represents depth-induced and current-induced refraction. The quantities c_σ and c_θ are the propagation velocities in spectral space (σ, θ). The right-hand

side contains S_{tot}, which is the source/sink term that represents all physical processes which generate, dissipate, or redistribute wave energy. They are defined for energy density $E(\sigma, \theta)$. Details are given in Section 2.3.

The second term in Eq. 2.16 can be recasted in Cartesian, spherical or curvilinear co-ordinates. For small scale applications the spectral action balance equation may be expressed in Cartesian co-ordinates as given by

$$\frac{\partial N}{\partial t} + \frac{\partial c_x N}{\partial x} + \frac{\partial c_y N}{\partial y} + \frac{\partial c_\sigma N}{\partial \sigma} + \frac{\partial c_\theta N}{\partial \theta} = \frac{S_{\text{tot}}}{\sigma} \tag{2.17}$$

with

$$c_x = c_{g,x} + U_x\,, \quad c_y = c_{g,y} + U_y \tag{2.18}$$

With respect to applications at shelf sea or oceanic scales the action balance equation may be recasted in spherical co-ordinates as follows:

$$\frac{\partial N}{\partial t} + \frac{\partial c_\lambda N}{\partial \lambda} + \cos^{-1}\varphi \frac{\partial c_\varphi \cos\varphi N}{\partial \varphi} + \frac{\partial c_\sigma N}{\partial \sigma} + \frac{\partial c_\theta N}{\partial \theta} = \frac{S_{\text{tot}}}{\sigma} \tag{2.19}$$

with longitude, λ and latitude φ.

2.3 Sources and sinks

First, in Section 2.3.1 general concepts of the physical processes of generation, dissipation and non-linear wave-wave interactions that are implemented in SWAN are outlined. Next, complete expressions for these physical processes are given in subsequent sections.

2.3.1 General concepts

In shallow water, six processes contribute to S_{tot}:

$$S_{\text{tot}} = S_{\text{in}} + S_{\text{nl3}} + S_{\text{nl4}} + S_{\text{ds,w}} + S_{\text{ds,b}} + S_{\text{ds,br}}\,. \tag{2.20}$$

These terms denote, respectively, wave growth by the wind, nonlinear transfer of wave energy through three-wave and four-wave interactions and wave decay due to whitecapping, bottom friction and depth-induced wave breaking. First, a brief summary of the formulations is given below. Next, for each term complete expressions are outlined.

Wind input

Transfer of wind energy to the waves is described with a resonance mechanism (Phillips, 1957) and a feed-back mechanism (Miles, 1957).

Resonance with wind-induced pressure fluctations

The pressure distribution induced by wind at the sea surface is random. It propagates more or less a frozen pattern over the surface with wind speed. This can be Fourier transformed to produce harmonic pressure waves that propagate with wind speed. If this harmonic pressure wave remains in phase with a free harmonic surface wave, then the wind energy is transferred from the pressure wave to the surface wave. The energy input by this mechanism, which contributes to the initial stages of wave growth, varies linearly with time.

Feedback of wave-induced pressure fluctations

When a wave has been generated by the resonance mechanism as explained above, it will distort the wind profile just above the water surface. This distortion results in an 'over pressure' on the wind ward side of the crest of the wave and an 'under pressure' at the lee side of the crest. It means that when the sea surface moves up and down, the pressure also follows the same movements, therefore transfer energy to the wave. This energy transfer is proportional to the energy in the wave itself, so the wave grows more as it gets larger. This effect is found to be exponential in time.

Based on the two wave growth mechanisms, wave growth due to wind commonly described as the sum of linear and exponential growth term of a wave component:

$$S_{\text{in}}(\sigma,\theta) = A + BE(\sigma,\theta) \tag{2.21}$$

in which A and B depend on wave frequency and direction, and wind speed and direction. The effects of currents are accounted for by using the apparent local wind speed and direction. The expression for the term A is due to Cavaleri and Malanotte-Rizzoli (1981) with a filter to avoid growth at frequencies lower than the Pierson-Moskowitz frequency (Tolman, 1992a). Two optional expressions for the coefficient B are used in the SWAN model. The first is taken from an early version of the WAM Cycle 3 model (the WAMDI group, 1988). It is due to Snyder *et al.* (1981), rescaled in terms of friction

velocity U_* by Komen *et al.* (1984). The drag coefficient to relate U_* to the driving wind speed at 10 m elevation U_{10} is taken from Wu (1982). The second expression for B in SWAN is taken from the WAM Cycle 4 model (Komen *et al.*, 1994). It is due to Janssen (1991a) and it accounts explicitly for the interaction between the wind and the waves by considering atmospheric boundary layer effects and the roughness length of the sea surface. The corresponding set of equations is solved (as in the WAM model) with the iterative procedure of Mastenbroek *et al.* (1993).

Dissipation

The dissipation term of wave energy is represented by the summation of three different contributions: whitecapping $S_{\mathrm{ds,w}}$, bottom friction $S_{\mathrm{ds,b}}$ and depth-induced breaking $S_{\mathrm{ds,br}}$.

Whitecapping is primarily controlled by the steepness of the waves. In presently operating third-generation wave models, the whitecapping formulations are based on a pulse-based model (Hasselmann, 1974), as adapted by the WAMDI group (1988):

$$S_{\mathrm{ds,w}}(\sigma,\theta) = -\Gamma\tilde{\sigma}\frac{k}{\tilde{k}}E(\sigma,\theta) \tag{2.22}$$

where Γ is a steepness dependent coefficient, k is wave number and $\tilde{\sigma}$ and $\tilde{k}$ denote a mean frequency and a mean wave number, respectively (cf. the WAMDI group, 1988). Komen *et al.* (1984) estimated the value of Γ by closing the energy balance of the waves in fully developed conditions. This implies that this value depends on the wind input formulation that is used. Since two expressions are used for the wind input in SWAN, also two values for Γ are used. The first is due to Komen *et al.* (1984), as in WAM Cycle 3. The second expression is an adaptation of this expression based on Janssen (1991a), as in WAM Cycle 4 (see Janssen, 1991b; Günther *et al.*, 1992). Young and Banner (1992) and Banner and Young (1994) have shown that the results of closing the energy balance in this manner depend critically on the choice of a high-frequency cut-off frequency above which a diagnostic spectral tail is used. In SWAN, this cut-off frequency is different from the one used in the WAM model. Differences in the growth rates between the WAM model and SWAN are therefore to be expected.

A number of alternative whitecapping expressions have been proposed to im-

prove the accuracy of SWAN. These range from alternative calibrations of the Komen *et al* (1984) expression, e.g. Rogers *et al* (2003), to alternative ways of calculating mean spectral steepness, e.g. Van Vledder and Hurdle (2002). In SWAN, two alternatives are presented.

An alternative formulation for whitecapping is based on the Cumulative Steepness Method as described in Hurdle and Van Vledder (2004). With this method dissipation due to whitecapping depends on the steepness of the wave spectrum at and below a particular frequency.

A second alternative of the whitecapping expression is based on Alves and Banner (2003). This expression is based on experimental findings that whitecapping dissipation appears to be related to the nonlinear hydrodynamics within wave groups. This yields a dissipation term that primarily depends on quantities that are local in the frequency spectrum, as opposed to ones that are distributed over the spectrum, as in the expression of Komen *et al* (1984). However, the final whitecapping expression proposed by Alves and Banner (2003) features additional dependencies on the spectral mean wavenumber and steepness, which is problematic in situations of mixed sea and swell often encountered in the nearshore. Therefore, their whitecapping expression is applied here without these mean spectral dependencies. This adapted whitecapping expression is used together with a wind input term that is based on that of Yan (1987). Further information and details can be found in Van der Westhuysen *et al* (2006).

In shallow water the orbital motions of the water particles, induced by surface waves, extend down to the sea floor. This gives rise to an interaction between te surface waves and the bottom. An overview of different wave-bottom interaction mechanisms and of their relative strengths is given by Shemdin *et al.* (1978). They are: scattering on bottom irregularities, motion of a soft bottom, percolation into a porous bottom and friction in the turbulent bottom boundary layer. The first process results in a local redistribution of wave energy by scattering of wave components. The last three are dissipative. Their strength depends on the bottom conditions. For continental shelf seas with sandy bottoms, the dominant mechanism appears to be bottom friction (Bertotti and Cavaleri, 1994) which can generally be expressed as:

$$S_{\mathrm{ds,b}} = -C_{\mathrm{b}} \frac{\sigma^2}{g^2 \sinh^2 kd} E(\sigma, \theta) \tag{2.23}$$

in which C_b is a bottom friction coefficient. A large number of models has been proposed since the pioneering paper of Putnam and Johnson (1949). Hasselmann *et al.* (1973) suggested to use an empirically obtained constant. It seems to perform well in many different conditions as long as a suitable value is chosen (typically different for swell and wind sea). A nonlinear formulation based on drag has been proposed by Hasselmann and Collins (1968) which was later simplified by Collins (1972). More complicated, eddy viscosity models have been developed by Madsen *et al.* (1988) and by Weber (1989, 1991a, 1991b). Considering the large variations in bottom conditions in coastal areas (bottom material, bottom roughness length, ripple height, etc.), there is no field data evidence to give preference to a particular friction model (Luo and Monbaliu, 1994). For this reason, the simplest of each of these types of friction models has been implemented in SWAN: the empirical JONSWAP model of Hasselmann *et al.* (1973), the drag law model of Collins (1972) and the eddy-viscosity model of Madsen *et al.* (1988). The effect of a mean current on the wave energy dissipation due to bottom friction is not taken into account in SWAN. The reasons for this are given by Tolman (1992b) who argues that state-of-the-art expressions vary too widely in their effects to be acceptable. He found that the error in finding a correct estimate of the bottom roughness length scale has a much larger impact on the energy dissipation rate than the effect of a mean current.

When waves propagate towards shore, shoaling leads to an increase in wave height. When the ratio of wave height over water depth exceeds a certain limit, waves start to break, thereby dissipating energy rapidly. In extreme shallow water (surf zone), this process becomes dominant over all other processes. The process of depth-induced wave breaking is still poorly understood and little is known about its spectral modelling. In contrast to this, the total dissipation (i.e. integrated over the spectral space) due to this type of wave breaking can be well modelled with the dissipation of a bore applied to the breaking waves in a random field (Battjes and Janssen, 1978; Thornton and Guza, 1983). Laboratory observations (e.g., Battjes and Beji, 1992; Vincent *et al.* 1994; Arcilla *et al.*, 1994 and Eldeberky and Battjes, 1996) show that the shape of initially uni-modal spectra propagating across simple (barred) beach profiles, is fairly insensitive to depth-induced breaking. This has led Eldeberky and Battjes (1995) to formulate a spectral version of the bore model of Battjes and Janssen (1978) that conserves the spectral shape.

Expanding their expression to include directions, the expression reads:

$$S_{\mathrm{ds,br}}(\sigma,\theta) = \frac{D_{\mathrm{tot}}}{E_{\mathrm{tot}}} E(\sigma,\theta) \tag{2.24}$$

in which E_{tot} is the total wave energy and $D_{\mathrm{tot}} < 0$ is the rate of dissipation of the total energy due to wave breaking according to Battjes and Janssen (1978). Adding a quadratic dependency on frequency as suggested by Mase and Kirby (1992) and supported by Elgar *et al.* (1997) seems to have no noticeable effect on the SWAN results. Chen and Guza (1997) inferred from observations and simulations with a Boussinesq model that the high-frequency levels are insensitive to such frequency dependency because an increased dissipation at high frequencies is compensated approximately by increased nonlinear energy transfer (but they did find the frequency dependency to be relevant in time domain). The value of D_{tot} depends critically on the breaking parameter $\gamma = H_{\mathrm{max}}/d$ (in which H_{max} is the maximum possible individual wave height in the local water depth d). In SWAN, both a constant value and a variable value are available. The constant value is $\gamma = 0.73$ found as the mean value of the data set of Battjes and Stive (1985).

Nonlinear wave-wave interactions

The basic properties of wave-wave interactions were discovered during the fundamental research of Phillips (1960) and Hasselmann (1960, 1962, 1963a,b). The physical meaning of the interactions is that resonant sets of wave components exchange energy, redistributing energy over the spectrum. In deep and intermediate water, four-wave interactions (so-called quadruplets) are important, whereas in shallow water three-wave interactions (so-called triads) become important.

In deep water, quadruplet wave-wave interactions dominate the evolution of the spectrum. They transfer wave energy from the spectral peak to lower frequencies (thus moving the peak frequency to lower values) and to higher frequencies (where the energy is dissipated by whitecapping). In very shallow water, triad wave-wave interactions transfer energy from lower frequencies to higher frequencies often resulting in higher harmonics (Beji and Battjes, 1993). Low-frequency energy generation by triad wave-wave interactions is not considered here.

A full computation of the quadruplet wave-wave interactions is extremely time consuming and not convenient in an operational wave model. Nevertheless, SWAN has two options to compute the Boltzmann integral in an exact manner. The first approach is the so-called FD-RIAM technique as proposed by Hashimoto *et al.* (1998). This approach enables to capture the frequency shift and the spectral shape changes as water depth decreases. The second approach is the exact method developed by Webb, Tracy and Resio (WRT) (Resio *et al.*, 2001). This algorithm was reprogrammed by Van Vledder, bearing the name XNL (Van Vledder and Bottema, 2003). This method is also enable to capture the frequency shift and the spectral shape changes as water depth decreases.

A number of techniques, based on parametric methods and approximations have been proposed to improve computational speed of computing quadruplets (see Young and Van Vledder (1993) for a review). In SWAN, the computations are carried out with the Discrete Interaction Approximation (DIA) of Hasselmann *et al.* (1985). This DIA has been found to be quite successful in describing the essential features of a developing wave spectrum; see Komen *et al.* (1994). For uni-directional waves, this approximation is not valid. In fact, the quadruplet interaction coefficient for these waves is nearly zero. For finite-depth applications, Hasselmann and Hasselmann (1981) have shown that for a JONSWAP-type spectrum the quadruplet wave-wave interactions can be scaled with a simple expression. In some cases, the DIA technique may not be accurate enough. In Hashimoto *et al.* (2003), it was demonstrated that the accuracy of the DIA may be improved by increasing the number of quadruplet configurations. They proposed a Multiple DIA with up to 6 wave number configurations.

In very shallow water, triad wave interactions become important for steep waves. It transfers energy to higher frequencies, resulting in higher harmonics (Beji and Battjes, 1993). The energy transfer in this process can take place over relatively short distance and can dramatically change single peaked spectra into multiple peaked spectra, which has frequently been observed in the field (Arcilla *et al.*, 1994) and in a number of laboratory experiments with a bar-trough profile (Beji and Battjes, 1993) and a plane beach profile (Nwogu, 1994).

A first attempt to describe triad wave-wave interactions in terms of a spectral

energy source term was made by Abreu *et al.* (1992). However, their expression is restricted to non-dispersive shallow water waves and is therefore not suitable in many practical applications of wind waves. The breakthrough in the development came with the work of Eldeberky and Battjes (1995) who transformed the amplitude part of the Boussinesq model of Madsen and Sørensen (1993) into an energy density formulation and who parameterized the bi-phase of the waves on the basis of laboratory observations (Battjes and Beji, 1992; Arcilla *et al.*, 1994). A discrete triad approximation (DTA) for co-linear waves was subsequently obtained by considering only the dominant self-self interactions. Their model has been verified with flume observations of long-crested, random waves breaking over a submerged bar (Beji and Battjes, 1993) and over a barred beach (Arcilla *et al.*, 1994). The model appeared to be fairly successful in describing the essential features of the energy transfer from the primary peak of the spectrum to the super harmonics. A slightly different version, the so-called Lumped Triad Approximation (LTA) was later derived by Eldeberky (1996). This LTA technique is employed in SWAN.

2.3.2 Input by wind (S_{in})

Wave growth by wind is described by:

$$S_{\text{in}}(\sigma,\theta) = A + BE(\sigma,\theta) \tag{2.25}$$

in which A describes linear growth and BE exponential growth. It should be noted that the SWAN model is driven by the wind speed at 10m elevation U_{10} whereas it uses the friction velocity U_*. For the WAM Cycle 3 formulation the transformation from U_{10} to U_* is obtained with

$$U_*^2 = C_D U_{10}^2 \tag{2.26}$$

in which C_D is the drag coefficient from Wu (1982):

$$C_D(U_{10}) = \begin{cases} 1.2875 \times 10^{-3}\,, & \text{for } U_{10} < 7.5 m/s \\ (0.8 + 0.065 s/m \times U_{10}) \times 10^{-3}\,, & \text{for } U_{10} \geq 7.5 m/s \end{cases} \tag{2.27}$$

For the WAM Cycle 4 formulations, the computation of U_* is an integral part of the source term.

Linear growth by wind

For the linear growth term A, the expression due to Cavaleri and Malanotte-Rizzoli (1981) is used with a filter to eliminate wave growth at frequencies lower than the Pierson-Moskowitz frequency (Tolman, 1992a)[1]:

$$A = \frac{1.5 \times 10^{-3}}{2\pi g^2}(U_* \max[0, \cos(\theta - \theta_w)])^4 H \,, \quad H = \exp\left\{-(\frac{\sigma}{\sigma^*_{\rm PM}})^{-4}\right\}, \quad \sigma^*_{\rm PM} = \frac{0.13g}{28U_*}2\pi \tag{2.28}$$

in which θ_w is the wind direction, H is the filter and $\sigma^*_{\rm PM}$ is the peak frequency of the fully developed sea state according to Pierson and Moskowitz (1964) as reformulated in terms of friction velocity.

Exponential growth by wind

Two expressions for exponential growth by wind are optionally available in the SWAN model. The first expression is due to Komen *et al.* (1984). Their expression is a function of $U_*/c_{\rm ph}$:

$$B = \max[0, 0.25\frac{\rho_a}{\rho_w}(28\frac{U_*}{c_{\rm ph}}\cos(\theta - \theta_w) - 1)]\sigma \tag{2.29}$$

in which $c_{\rm ph}$ is the phase speed and ρ_a and ρ_w are the density of air and water, respectively. This expression is also used in WAM Cycle 3 (the WAMDI group, 1988). The second expression is due to Janssen (1989,1991a). It is based on a quasi-linear wind-wave theory and is given by:

$$B = \beta\frac{\rho_a}{\rho_w}\left(\frac{U_*}{c_{\rm ph}}\right)^2 \max[0, \cos(\theta - \theta_w)]^2\sigma \tag{2.30}$$

where β is the Miles constant. In the theory of Janssen (1991a), this constant is estimated from the non-dimensional critical height λ:

$$\begin{cases} \beta = \frac{1.2}{\kappa^2}\lambda \ln^4 \lambda \,, & \lambda \leq 1 \\ \lambda = \frac{gz_e}{c^2_{\rm ph}}e^r \,, & r = \kappa c/|U_* \cos(\theta - \theta_w)| \end{cases} \tag{2.31}$$

where $\kappa = 0.41$ is the Von Karman constant and z_e is the effective surface roughness. If the non-dimensional critical height $\lambda > 1$, the Miles constant

[1] In Eq. (10) of Tolman (1992a) the power of 10^{-5} should be 10^{-3}; H. Tolman, personal communication, 1995.

β is set equal 0. Janssen (1991a) assumes that the wind profile is given by:

$$U(z) = \frac{U_*}{\kappa} \ln[\frac{z + z_e - z_0}{z_e}] \tag{2.32}$$

in which $U(z)$ is the wind speed at height z (10m in the SWAN model) above the mean water level, z_0 is the roughness length. The effective roughness length z_e depends on the roughness length z_0 and the sea state through the wave-induced stress $\vec{\tau_w}$ and the total surface stress $\vec{\tau} = \rho_a |\vec{U_*}| \vec{U_*}$:

$$z_e = \frac{z_0}{\sqrt{1 - \frac{|\vec{\tau_w}|}{|\vec{\tau}|}}}, \quad z_0 = \hat{\alpha} \frac{U_*^2}{g} \tag{2.33}$$

The second of these two equations is a Charnock-like relation in which $\hat{\alpha}$ is a constant equal to 0.01. The wave stress $\vec{\tau}_w$ is given by:

$$\vec{\tau}_w = \rho_w \int_0^{2\pi} \int_0^{\infty} \sigma B E(\sigma, \theta) \frac{\vec{k}}{k} d\sigma d\theta \tag{2.34}$$

The value of U_* can be determined for a given wind speed U_{10} and a given wave spectrum $E(\sigma, \theta)$ from the above set of equations. In the SWAN model, the iterative procedure of Mastenbroek *et al.* (1993) is used. This set of expressions (2.30) through (2.34) is also used in WAM Cycle 4 (Komen *et al.*, 1994).

2.3.3 Dissipation of wave energy (S_{ds})

Whitecapping: Komen *et al* (1984) formulation

The processes of whitecapping in the SWAN model is represented by the pulse-based model of Hasselmann (1974). Reformulated in terms of wave number (rather than frequency) so as to be applicable in finite water depth (cf. the WAMDI group, 1988), this expression is:

$$S_{\mathrm{ds,w}}(\sigma, \theta) = -\Gamma \tilde{\sigma} \frac{k}{\tilde{k}} E(\sigma, \theta) \tag{2.35}$$

where $\tilde{\sigma}$ and $\tilde{k}$ denote the mean frequency and the mean wave number, respectively, and the coefficient Γ depends on the overall wave steepness. This steepness dependent coefficient, as given by the WAMDI group (1988), has

been adapted by Günther *et al.* (1992) based on Janssen (1991a) (see also (Janssen, 1991b)):

$$\Gamma = \Gamma_{\mathrm{KJ}} = C_{\mathrm{ds}}((1-\delta) + \delta\frac{k}{\tilde{k}}) \left(\frac{\tilde{s}}{\tilde{s}_{\mathrm{PM}}}\right)^{p} \tag{2.36}$$

For $\delta = 0$ the expression of Γ reduces to the expression as used by the WAMDI group (1988). The coefficients C_{ds}, δ and p are tunable coefficients, $\tilde{s}$ is the overall wave steepness, $\tilde{s}_{\mathrm{PM}}$ is the value of $\tilde{s}$ for the Pierson-Moskowitz spectrum (1964): $\tilde{s}_{PM} = \sqrt{3.02 \times 10^{-3}}$. The overall wave steepness $\tilde{s}$ is defined as:

$$\tilde{s} = \tilde{k}\sqrt{E_{\mathrm{tot}}} \tag{2.37}$$

The mean frequency $\tilde{\sigma}$, the mean wave number $\tilde{k}$ and the total wave energy E_{tot} are defined as (cf. the WAMDI group, 1988):

$$\tilde{\sigma} = \left(E_{\mathrm{tot}}^{-1} \int_0^{2\pi} \int_0^{\infty} \frac{1}{\sigma} E(\sigma,\theta) d\sigma d\theta\right)^{-1} \tag{2.38}$$

$$\tilde{k} = \left(E_{\mathrm{tot}}^{-1} \int_0^{2\pi} \int_0^{\infty} \frac{1}{\sqrt{k}} E(\sigma,\theta) d\sigma d\theta\right)^{-2} \tag{2.39}$$

$$E_{\mathrm{tot}} = \int_0^{2\pi} \int_0^{\infty} E(\sigma,\theta) d\sigma d\theta \tag{2.40}$$

The values of the tunable coefficients C_{ds} and δ and exponent p in this model have been obtained by Komen *et al.* (1984) and Janssen (1992) by closing the energy balance of the waves in idealized wave growth conditions (both for growing and fully developed wind seas) for deep water. This implies that coefficients in the steepness dependent coefficient Γ depend on the wind input formulation that is used. Since two different wind input formulations are used in the SWAN model, two sets of coefficients are used. For the wind input of Komen *et al.* (1984; corresponding to WAM Cycle 3; the WAMDI group, 1988): $C_{\mathrm{ds}} = 2.36 \times 10^{-5}$, $\delta = 0$ and $p = 4$. Janssen (1992) and also Günther *et al* (1992) obtained (assuming $p = 4$) $C_{\mathrm{ds}} = 4.10 \times 10^{-5}$ and $\delta = 0.5$ (as used in the WAM Cycle 4; Komen *et al.*, 1994).

Whitecapping: CSM formulation

An alternative formulation for whitecapping is based on the Cumulative Steepness Method as described in Hurdle and Van Vledder (2004). With

this method dissipation due to whitecapping depends on the steepness of the wave spectrum at and below a particular frequency. It is defined as (directionally dependent):

$$S_{\mathrm{st}}(\sigma,\theta) = A_m \int_0^{\sigma}\int_0^{2\pi} k^2 |\cos(\theta-\theta')|^m E(\sigma,\theta) d\sigma d\theta \tag{2.41}$$

with A_m the normalisation coefficient as determined by

$$\int_0^{2\pi} A_m \cos^m(\theta) d\theta = 1 \tag{2.42}$$

In expression (2.41) the coefficient m controls the directional dependence. It is expected that this coefficient will be order 1 if the straining mechanism is dominant, m is more than 10 if other mechanism play a role (e.g. instability that occurs when vertical acceleration in the waves becomes greater than gravity). Default in SWAN is $m = 2$. The alternative whitecapping source term is given by

$$S_{\mathrm{wc}}^{\mathrm{st}} = -C_{\mathrm{wc}}^{\mathrm{st}} \left(S_{\mathrm{st}}(\sigma,\theta)\right)^p E(\sigma,\theta) \tag{2.43}$$

with C_{wc}^{st} a tuneable coefficient and p a parameter controlling the proportionality of the dissipation rate on the steepness. In SWAN, $p = 1$ is assumed.

Whitecapping: saturation-based model

The whitecapping formulation used in SWAN is an adapted form of the expression of Alves and Banner (2003), which is based on the apparent relationship between wave groups and whitecapping dissipation. This adaption is due to the fact that it can also be applied to mixed sea-swell conditions and in shallow water. This was done by removing the dependencies on mean spectral steepness and wavenumber in the original expression, and by applying source term scaling arguments for its calibration (see below). This led to the following expression for whitecapping dissipation

$$S_{\mathrm{ds,w}}(\sigma,\theta) = -C_{\mathrm{ds}} \left(\frac{B(k)}{B_{\mathrm{r}}}\right)^{p/2} (\tanh(kh))^{(2-p_0)/4} \sqrt{gk} E(\sigma,\theta) \tag{2.44}$$

in which the density function $B(k)$ is the azimuthal-integrated spectral saturation, which is positively correlated with the probability of wave group-induced breaking. It is calculated from frequency space variables as follows

$$B(k) = \int_0^{2\pi} c_g k^3 E(\sigma,\theta) d\theta \tag{2.45}$$

and B_r is a threshold saturation level. When $B(k) > B_\mathrm{r}$, waves break and the exponent p is set equal to a calibration parameter p_0. For $B(k) \leq B_\mathrm{r}$ there is no breaking, but some residual dissipation proved necessary. This is obtained by setting $p = 0$. A smooth transition between these two situations is achieved by (Alves and Banner, 2003);

$$p = \frac{p_0}{2} + \frac{p_0}{2} \tanh \left[10 \left(\sqrt{\frac{B(k)}{B_\mathrm{r}}} - 1 \right) \right] \tag{2.46}$$

The wind input expression used in saturation-based model is based on that by Yan (1987). This expression embodies experimental findings that for strong wind forcing, $u_*/c > 0.1$ say, the wind-induced growth rate of waves depends quadratically on u_*/c (e.g. Plant 1982), whereas for weaker forcing, $u_*/c < 0.1$ say, the growth rate depends linearly on u_*/c (Snyder *et al*, 1981). Yan (1987) proposes an analytical fit through these two ranges of the form:

$$\beta_\mathrm{fit} = D \left(\frac{u_*}{c} \right)^2 \cos(\theta - \alpha) + E \left(\frac{u_*}{c} \right) \cos(\theta - \alpha) + F \cos(\theta - \alpha) + H \tag{2.47}$$

where D,E,F and H are coefficients of the fit. Yan imposed two constraints:

$$\beta_\mathrm{fit} \approx \beta_\mathrm{Snyder} \quad \text{for} \quad \frac{U_5}{c} \approx 1 \ \ (\text{or } \frac{u_*}{c} \approx 0.036) \tag{2.48}$$

and

$$\lim_{u_*/c \to \infty} \beta_\mathrm{fit} = \beta_\mathrm{Plant} \tag{2.49}$$

in which β_Snyder and β_Plant are the growth rates proposed by Snyder *et al* (1981) and Plant (1982), respectively. Application of Eqs. (2.48) and (2.49) led us to parameter values of $D = 4.0 \times 10^{-2}$,$E = 5.52 \times 10^{-3}$,$F = 5.2 \times 10^{-5}$ and $H = -3.02 \times 10^{-4}$, which are somewhat different from those proposed by Yan (1987). We found that our parameter values produce better fetch-limited simulation results in the Pierson and Moskowitz (1964) fetch range thant the original values of Yan (1987).

Finally, the choice of the exponent p_0 in Eqs. (2.44) and (2.46) is made by requiring that the source terms of whitecapping (Eq. 2.44) and wind input (Eq. 2.47) have equal scaling in frequency, after Resio *et al* (2004). This leads to a value of $p_0 = 4$ for strong wind forcing ($u_*/c > 0.1$) and $p_0 = 2$ for

weaker forcing ($u_*/c < 0.1$). A smooth transition between these two limits, centred around $u_*/c = 0.1$, is achieved by the expression

$$p_0(\sigma) = 3 + \tanh\left[w\left(\frac{u_*}{c} - 0.1\right)\right] \tag{2.50}$$

where w is a scaling parameter for which a value of $w = 26$ is used in SWAN. In shallow water, under strong wind forcing ($p_0 = 4$), this scaling condition requires the additional dimensionless factor $\tanh(kh)^{-1/2}$ in Eq. (2.44), where h is the water depth.

Bottom friction

The bottom friction models that have been selected for SWAN are the empirical model of JONSWAP (Hasselmann *et al.*, 1973), the drag law model of Collins (1972) and the eddy-viscosity model of Madsen *et al.* (1988). The formulations for these bottom friction models can all be expressed in the following form:

$$S_{\mathrm{ds,b}} = -C_{\mathrm{b}} \frac{\sigma^2}{g^2 \sinh^2 kd} E(\sigma,\theta) \tag{2.51}$$

in which C_{b} is a bottom friction coefficient that generally depends on the bottom orbital motion represented by U_{rms}:

$$U_{rms}^2 = \int_0^{2\pi}\int_0^{\infty} \frac{\sigma^2}{g^2 \sinh^2 kd} E(\sigma,\theta) d\sigma d\theta \tag{2.52}$$

Hasselmann *et al.* (1973) found from the results of the JONSWAP experiment $C_{\mathrm{b}} = C_{\mathrm{JON}} = 0.038\mathrm{m}^2\mathrm{s}^{-3}$ for swell conditions. Bouws and Komen (1983) selected a bottom friction coefficient of $C_{\mathrm{JON}} = 0.067\mathrm{m}^2\mathrm{s}^{-3}$ for fully developed wave conditions in shallow water. Both values are available in SWAN.

The expression of Collins (1972) is based on a conventional formulation for periodic waves with the appropriate parameters adapted to suit a random wave field. The dissipation rate is calculated with the conventional bottom friction formulation of Eq. (2.26) in which the bottom friction coefficient is $C_{\mathrm{b}} = C_f g U_{\mathrm{rms}}$ with $C_f = 0.015$ (Collins, 1972)[2].

[2]Collins (1972) contains an error in the expression due to an erroneous Jacobian transformation. See page A-16 of Tolman (1990).

Madsen *et al.* (1988) derived a formulation similar to that of Hasselmann and Collins (1968) but in their model the bottom friction factor is a function of the bottom roughness height and the actual wave conditions. Their bottom friction coefficient is given by:

$$C_{\mathrm{b}} = f_w \frac{g}{\sqrt{2}} U_{rms} \tag{2.53}$$

in which f_w is a non-dimensional friction factor estimated by using the formulation of Jonsson (1966) cf. Madsen *et al.* (1988):

$$\frac{1}{4\sqrt{f_w}} + \log_{10}(\frac{1}{4\sqrt{f_w}}) = m_f + \log_{10}(\frac{a_b}{K_{\mathrm{N}}}) \tag{2.54}$$

in which $m_f = -0.08$ (Jonsson and Carlsen, 1976) and a_b is a representative near-bottom excursion amplitude:

$$a_b^2 = 2 \int_0^{2\pi} \int_0^{\infty} \frac{1}{\sinh^2 kd} E(\sigma, \theta) d\sigma d\theta \tag{2.55}$$

and K_{N} is the bottom roughness length scale. For values of a_b/K_{N} smaller than 1.57 the friction factor f_w is 0.30 (Jonsson, 1980).

Depth-induced wave breaking

To model the energy dissipation in random waves due to depth-induced breaking, the bore-based model of Battjes and Janssen (1978) is used in SWAN. The mean rate of energy dissipation per unit horizontal area due to wave breaking D_{tot} is expressed as:

$$D_{\mathrm{tot}} = -\frac{1}{4} \alpha_{\mathrm{BJ}} Q_b (\frac{\tilde{\sigma}}{2\pi}) H_{\mathrm{max}}^2 = \alpha_{\mathrm{BJ}} Q_b \tilde{\sigma} \frac{H_{\mathrm{max}}^2}{8\pi} \tag{2.56}$$

in which $\alpha_{\mathrm{BJ}} = 1$ in SWAN, Q_b is the fraction of breaking waves determined by:

$$\frac{1 - Q_b}{\ln Q_b} = -8 \frac{E_{\mathrm{tot}}}{H_{\mathrm{max}}^2} \tag{2.57}$$

in which H_{max} is the maximum wave height that can exist at the given depth and $\tilde{\sigma}$ is a mean frequency defined as:

$$\tilde{\sigma} = E_{\mathrm{tot}}^{-1} \int_0^{2\pi} \int_0^{\infty} \sigma E(\sigma, \theta) d\sigma d\theta \tag{2.58}$$

The fraction of depth-induced breakers (Q_b) is determined in SWAN with

$$Q_b = \begin{cases} 0\,, & \text{for } \beta \leq 0.2 \\ Q_0 - \beta^2 \frac{Q_0 - \exp\left(Q_0 - 1\right)/\beta^2}{\beta^2 - \exp\left(Q_0 - 1\right)/\beta^2}\,, & \text{for } 0.2 < \beta < 1 \\ 1\,, & \text{for } \beta \geq 1 \end{cases} \tag{2.59}$$

where $\beta = H_{\rm rms}/H_{\rm max}$. Furthermore, for $\beta \leq 0.5$, $Q_0 = 0$ and for $0.5 < \beta \leq 1$, $Q_0 = (2\beta - 1)^2$.

Extending the expression of Eldeberky and Battjes (1995) to include the spectral directions, the dissipation for a spectral component per unit time is calculated in SWAN with:

$$S_{\rm ds,br}(\sigma,\theta) = \frac{D_{\rm tot}}{E_{\rm tot}} E(\sigma,\theta) = -\frac{\alpha_{\rm BJ} Q_b \tilde{\sigma}}{\beta^2 \pi} E(\sigma,\theta) \tag{2.60}$$

The maximum wave height $H_{\rm max}$ is determined in SWAN with $H_m = \gamma d$, in which γ is the breaker parameter and d is the total water depth (including the wave-induced set-up if computed by SWAN). In the literature, this breaker parameter γ is often a constant or it is expressed as a function of bottom slope or incident wave steepness (see e.g., Galvin, 1972; Battjes and Janssen, 1978; Battjes and Stive, 1985; Arcilla and Lemos, 1990; Kaminsky and Kraus, 1993; Nelson, 1987, 1994). In the publication of Battjes and Janssen (1978) in which the dissipation model is described, a constant breaker parameter, based on Miche's criterion, of $\gamma = 0.8$ was used. Battjes and Stive (1985) re-analyzed wave data of a number of laboratory and field experiments and found values for the breaker parameter varying between 0.6 and 0.83 for different types of bathymetry (plane, bar-trough and bar) with an average of 0.73. From a compilation of a large number of experiments Kaminsky and Kraus (1993) have found breaker parameters in the range of 0.6 to 1.59 with an average of 0.79.

2.3.4 Nonlinear wave-wave interactions ($S_{\rm nl}$)

Quadruplets

In this section two methods are described for the computation of non-linear interactions at deep water. The first method is called the DIA method and is

relatively crude in the approximation of the Boltzmann integral. The second one is called the XNL approach and is implemented in SWAN by G. Ph. van Vledder.

DIA

The quadruplet wave-wave interactions are computed with the Discrete Interaction Approximation (DIA) as proposed by Hasselmann *et al.* (1985). Their source code (slightly adapted by Tolman, personal communication, 1993) has been used in the SWAN model. In the DIA two quadruplets of wave numbers are considered, both with frequencies:

$$\sigma_1 = \sigma_2 = \sigma \,, \sigma_3 = \sigma(1+\lambda) = \sigma^+ \,, \sigma_4 = \sigma(1-\lambda) = \sigma^- \tag{2.61}$$

where λ is a constant coefficient set equal to 0.25. To satisfy the resonance conditions for the first quadruplet, the wave number vectors with frequency σ_3 and σ_4 lie at an angle of $\theta_1 = -11.5^o$ and $\theta_2 = 33.6^o$ to the two identical wave number vectors with frequencies σ_1 and σ_2. The second quadruplet is the mirror of this first quadruplet (the wave number vectors with frequency σ_3 and σ_4 lie at mirror angles of $\theta_3 = 11.5^o$ and $\theta_4 = -33.6^o$.

Within this discrete interaction approximation, the source term $S_{\rm nl4}(\sigma,\theta)$ is given by:

$$S_{\rm nl4}(\sigma,\theta) = S^{*}_{\rm nl4}(\sigma,\theta) + S^{**}_{\rm nl4}(\sigma,\theta) \tag{2.62}$$

where $S^{*}_{\rm nl4}$ refers to the first quadruplet and $S^{**}_{\rm nl4}$ to the second quadruplet (the expressions for $S^{**}_{\rm nl4}$ are identical to those for $S^{*}_{\rm nl4}$ for the mirror directions) and:

$$S^{*}_{\rm nl4} = 2\delta S_{\rm nl4}(\alpha_1\sigma,\theta) - \delta S_{\rm nl4}(\alpha_2\sigma,\theta) - \delta S_{\rm nl4}(\alpha_3\sigma,\theta) \tag{2.63}$$

in which $\alpha_1 = 1$, $\alpha_2 = (1+\lambda)$ and $\alpha_3 = (1-\lambda)$. Each of the contributions $(i = 1,2,3)$ is:

$$\begin{aligned}\delta S_{\rm nl4}(\alpha_i\sigma,\theta) \;=\; & C_{\rm nl4}(2\pi)^2 g^{-4}\left(\frac{\sigma}{2\pi}\right)^{11}\left[E^2(\alpha_i\sigma,\theta)\left\{\frac{E(\alpha_i\sigma^+,\theta)}{(1+\lambda)^4}+\frac{E(\alpha_i\sigma^-,\theta)}{(1-\lambda)^4}\right\}\right. \\ & \left. -2\frac{E(\alpha_i\sigma,\theta)E(\alpha_i\sigma^+,\theta)E(\alpha_i\sigma^-,\theta)}{(1-\lambda^2)^4}\right]\end{aligned} \tag{2.64}$$

with constant $C_{nl4} = 3\times 10^7$. Following Hasselmann and Hasselmann (1981), the quadruplet interaction in finite water depth is taken identical to the

quadruplet transfer in deep water multiplied with a scaling factor:

$$S_{\mathrm{nl4}}^{\text{finite depth}} = R(k_p d) S_{\mathrm{nl4}}^{\text{deep water}} \tag{2.65}$$

where R is given by:

$$R(k_p d) = 1 + \frac{C_{sh1}}{k_p d}(1 - C_{sh2} k_p d) e^{C_{sh3} k_p d} \tag{2.66}$$

in which k_p is the peak wave number of the JONSWAP spectrum for which the original computations were carried out. The values of the coefficients are: $C_{sh1} = 5.5$, $C_{sh2} = 6/7$ and $C_{sh3} = -1.25$. In the shallow water limit, i.e., $k_p \to 0$ the nonlinear transfer tends to infinity. Therefore, a lower limit of $k_p = 0.5$ is applied (cf. WAM Cycle 4; Komen *et al.*, 1994), resulting in a maximum value of $R(k_p d) = 4.43$. To increase the model robustness in case of arbitrarily shaped spectra, the peak wave number k_p is replaced by $k_p = 0.75\tilde{k}$ (cf. Komen *et al.*, 1994).

XNL (G. Ph. van Vledder)

The second method for calculating the nonlinear interactions in SWAN is the so-called Webb-Resio-Tracy method (WRT), which is based on the original six-dimensional Boltzmann integral formulation of Hasselmann (1962, 1963a,b), and additional considerations by Webb (1978), Tracy and Resio (1982) and Resio and Perrie (1991). A detailed description of the WRT method and its implementation in discrete spectral wave models like SWAN is given in Van Vledder (2006). An overview of computational methods for computing the exact non-linear transfer rate is given in Benoit (2005).

The Boltzmann integral describes the rate of change of action density of a particular wave number due to resonant interactions between pairs of four wave numbers. To interact these wave numbers must satisfy the following resonance conditions

$$\left.\begin{array}{rcl} \vec{k}_1 + \vec{k}_2 &=& \vec{k}_3 + \vec{k}_4 \\ \sigma_1 + \sigma_2 &=& \sigma_3 + \sigma_4 \end{array}\right\} \quad . \tag{2.67}$$

The rate of change of action density N_1 at wave number $\vec{k}_1$ due to all quadruplet interactions involving $\vec{k}_1$ is given by

$$\begin{aligned} \frac{\partial N_1}{\partial t} &= \iiint G\left(\vec{k}_1, \vec{k}_2, \vec{k}_3, \vec{k}_4\right) \delta\left(\vec{k}_1 + \vec{k}_2 - \vec{k}_3 - \vec{k}_4\right) \delta\left(\sigma_1 + \sigma_2 - \sigma_3 - \sigma_4\right) \\ &\times \left[N_1 N_3 \left(N_4 - N_2\right) + N_2 N_4 \left(N_3 - N_1\right)\right] d\vec{k}_2\, d\vec{k}_3\, d\vec{k}_4 \quad , \end{aligned} \tag{2.68}$$

where the action density N is defined in terms of the wave number vector $\vec{k}$, $N = N(\vec{k})$. The term G is a complicated coupling coefficient for which an explicit expression has been given by Herterich and Hasselmann (1980). In the WRT method a number of transformations are made to remove the delta functions. A key element in the WRT method is to consider the integration space for each $(\vec{k}_1, \vec{k}_3)$ combination

$$\frac{\partial N_1}{\partial t} = 2 \int T\left(\vec{k}_1, \vec{k}_3\right)\, d\vec{k}_3 \quad , \tag{2.69}$$

in which the function T is given by

$$\begin{aligned} T\left(\vec{k}_1, \vec{k}_3\right) &= \iint G\left(\vec{k}_1, \vec{k}_2, \vec{k}_3, \vec{k}_4\right)\, \delta\left(\vec{k}_1 + \vec{k}_2 - \vec{k}_3 - \vec{k}_4\right) \\ &\times \delta\left(\sigma_1 + \sigma_2 - \sigma_3 - \sigma_4\right)\, \theta\left(\vec{k}_1, \vec{k}_3, \vec{k}_4\right) \\ &\times \left[N_1 N_3 \left(N_4 - N_2\right) + N_2 N_4 \left(N_3 - N_1\right)\right]\, d\vec{k}_2\, d\vec{k}_4 \quad , \end{aligned} \tag{2.70}$$

in which

$$\theta\left(\vec{k}_1, \vec{k}_3, \vec{k}_4\right) = \begin{cases} 1 & \text{when} \quad \left|\vec{k}_1 - \vec{k}_3\right| \leq \left|\vec{k}_1 - \vec{k}_4\right| \\ 0 & \text{when} \quad \left|\vec{k}_1 - \vec{k}_3\right| > \left|\vec{k}_1 - \vec{k}_4\right| \end{cases} \tag{2.71}$$

The delta functions in Eq. (2.70) determine a region in wave number space along which the integration should be carried out. The function θ determines a section of the integral which is not defined due to the assumption that $\vec{k}_1$ is closer to $\vec{k}_3$ than $\vec{k}_2$. The crux of the Webb method consists of using a local coordinate system along a so-named locus, that is, the path in $\vec{k}$ space that satisfies the resonance conditions for a given combination of $\vec{k}_1$ and $\vec{k}_3$. To that end the (k_x, k_y) coordinate system is replaced by a (s, n) coordinate system, where s (n) is the tangential (normal) direction along the locus. After some transformations the transfer integral can then be written as a closed line integral along the closed locus

$$\begin{aligned} T\left(\vec{k}_1, \vec{k}_3\right) &= \oint G\, J\, \theta(\vec{k}_1, \vec{k}_3, \vec{k}_4) \\ &\times \left[N_1 N_3 \left(N_4 - N_2\right) + N_2 N_4 \left(N_3 - N_1\right)\right]\, ds \quad , \end{aligned} \tag{2.72}$$

in which G is the coupling coefficient and J is the Jacobian term of a function representing the resonance conditions. The Jacobian term is a function of the group velocities of interacting wave numbers

$$J = \left|\vec{c}_{g,2} - \vec{c}_{g,4}\right|^{-1} \tag{2.73}$$

Numerically, the Boltzmann integral is computed as the finite sum of many line integrals T for all discrete combinations of $\vec{k}_1$ and $\vec{k}_3$. The line integral (2.72) is solved by dividing the locus in typically 40 pieces, such that it's discretized version is given as:

$$T\left(\vec{k}_1, \vec{k}_3\right) \approx \sum_{i=1}^{n_s} G(s_i) J(s_i) P(s_i)\, \Delta s_i \quad , \tag{2.74}$$

in which $P(s_i)$ is the product term for a given point on the locus, n_s is the number of segments, s_i is the discrete coordinate along the locus, and Δs_i is the stepsize. Finally, the rate of change for a given wave number $\vec{k}_1$ is given by

$$\frac{\partial N(\vec{k}_1)}{\partial t} \approx \sum_{i_{k3}=1}^{n_k} \sum_{i_{\theta 3}=1}^{n_\theta} T(\vec{k}_1, \vec{k}_3)\, \Delta k_{i_{k3}}\, \Delta \theta_{i_{\theta 3}} \tag{2.75}$$

where n_k and n_θ are the discrete number of wave numbers and directions in the computational spectral grid, respectively. Note that although the spectrum is defined in terms of the vector wave number $\vec{k}$, the computational grid in a wave model is more conveniently defined in terms of the absolute wave number and wave direction (k, θ) to assure directional isotropy of the calculations. Taking all wave numbers $\vec{k}_1$ into account produces the complete source term due to nonlinear quadruplet wave-wave interactions. Details of the computation of a locus for a given combination of the wave numbers $\vec{k}_1$ and $\vec{k}_3$ can be found in Van Vledder (2006).

It is noted that these exact interaction calculations are extremely expensive, typically requiring 10^3 to 10^4 times more computational effort than the DIA. Presently, these calculations can therefore only be made for highly idealized test cases involving a limited spatial grid.

The nonlinear interactions according to the WRT method have been implemented in SWAN using portable subroutines. In this implementation, the computational grid of the WRT method is based to the discrete spectral grid of SWAN. The WRT method uses a $(\vec{k}, \theta)$ grid which is based on the (σ, θ) grid of SWAN. In addition, the WRT routines inherit the power of the parametric spectral tail as in the DIA. Choosing a higher resolution than the computational grid of SWAN for computing the nonlinear interactions is possible in theory, but this does not improve the results and is therefore not implemented.

Because nonlinear quadruplet wave-wave interactions at high frequencies are important, it is recommended to choose the maximum frequency of the wave model about six times the peak frequency of the spectra that are expected to occur in a wave model run. Note that this is important as the spectral grid determines the range of integration in Eq. (2.75). The recommended number of frequencies is about 40, with a frequency increment factor 1.07. The recommended directional resolution for computing the nonlinear interactions is about 10°. For specific purposes other resolutions may be used, and some testing with other resolutions may be needed.

An important feature of most algorithms for the evaluation of the Boltzmann integral is that the integration space can be pre-computed. In the initialization phase of the wave model the integration space, consisting of the discretized paths of all loci, together with the interaction coefficients and Jacobians, are computed and stored in a binary data file. For each discrete water depth such a data file is generated and stored in the work directory. The names of these data files consist of a keyword, "xnl4v5", followed by the keyword "*xxxxx*", with *xxxxx* the water depth in a certain unit (meters by default), or *99999* for deep water. The extension of the binary data file is "bqf" (of Binary Quadruplet File). If a BQF file exists, the program checks if this BQF file has been generated with the proper spectral grid. If this is not the case, a new BQF file is generated and the existing BQF file is overwritten. During a wave model run with various depths, the optimal BQF is used, by looking at the 'nearest' water depth d_N for which a valid BQF file has been generated. In addition, the result is rescaled using the DIA scaling (2.66) according to

$$S^{d}_{\mathrm{nl4}} = S^{d_N}_{\mathrm{nl4}} \frac{R(k_p d)}{R(k_p d_N)} \quad . \tag{2.76}$$

Triads

The Lumped Triad Approximation (LTA) of Eldeberky (1996), which is a slightly adapted version of the Discrete Triad Approximation (DTA) of Eldeberky and Battjes (1995) is used in SWAN in each spectral direction:

$$S_{\mathrm{nl3}}(\sigma,\theta) = S^{-}_{\mathrm{nl3}}(\sigma,\theta) + S^{+}_{\mathrm{nl3}}(\sigma,\theta) \tag{2.77}$$

with

$$S^{+}_{\mathrm{nl3}}(\sigma,\theta) = \max[0, \alpha_{\mathrm{EB}} 2\pi c c_g J^2 |\sin\beta| \left\{ E^2(\sigma/2,\theta) - 2E(\sigma/2,\theta)E(\sigma,\theta) \right\}] \tag{2.78}$$

and

$$S^{-}_{\mathrm{nl3}}(\sigma,\theta) = -2S^{+}_{\mathrm{nl3}}(2\sigma,\theta) \tag{2.79}$$

in which α_{EB} is a tunable proportionality coefficient. The bi-phase β is approximated with

$$\beta = -\frac{\pi}{2} + \frac{\pi}{2}\tanh(\frac{0.2}{Ur}) \tag{2.80}$$

with Ursell number Ur:

$$Ur = \frac{g}{8\sqrt{2}\pi^2}\frac{H_s {T_{m01}}^2}{d^2} \tag{2.81}$$

The triad wave-wave interactions are calculated only for $0 \leq Ur \leq 1$. The interaction coefficient J is taken from Madsen and Sørensen (1993):

$$J = \frac{k^2_{\sigma/2}(gd + 2c^2_{\sigma/2})}{k_\sigma d(gd + \frac{2}{15}gd^3k^2_\sigma - \frac{2}{5}\sigma^2 d^2)} \tag{2.82}$$

2.4 The influence of ambient current on waves

Waves are subject to the influence of ambient current, when they propagate on it. The ambient current can be tidal current, ocean current, local wind generated current, river current and wave generated current. It has been observed that current affects the growth and decay of waves (Yu, 1952; Hedges *et al.*, 1985; Lia *et al.*, 1989). The observations have shown that in a strong opposite current the wave steepness and wave height increase significantly. These changes take place rapidly where the waves are blocked by the current, often accompanied with current-induced whitecapping and wave reflections. Moreover, at the blocking frequency action is also partially transferred away from the blocking frequency to higher and lower frequencies by nonlinear wave-wave interactions (Ris, 1997).

It was Longuet-Higgins and Stewart (1960, 1961, 1962) who founded the theoretical description of wave-current interactions. Since then, many additional results of wave-current interactions have been published. If waves propagate

in the presence of ambient current, action density is conserved whereas energy density is not. Therefore, in SWAN the action balance equation has been adopted.

2.5 Modelling of obstacles

SWAN can estimate wave transmission through a (line-)structure such as a breakwater (dam). Such an obstacle will affect the wave field in two ways, first it will reduce the wave height locally all along its length, and second it will cause diffraction around its end(s). In irregular, short-crested wave fields, however, it seems that the effect of diffraction is small, except in a region less than one or two wavelengths away from the tip of the obstacle (Booij *et al.*, 1993). Therefore the model can reasonably account for waves around an obstacle if the directional spectrum of incoming waves is not too narrow. Since obstacles usually have a transversal area that is too small to be resolved by the bottom grid in SWAN, an obstacle is modelled as a line. If the crest of the breakwater is at a level where (at least part of the) waves can pass over, the transmission coefficient K_t (defined as the ratio of the (significant) wave height at the downwave side of the dam over the (significant) wave height at the upwave side) is a function of wave height and the difference in crest level and water level. The expression is taken from Goda *et al.* (1967):

$$K_t = 0.5(1 - \sin(\frac{\pi}{2\alpha}(\frac{F}{H_i} + \beta))) \ , \quad -\beta - \alpha < \frac{F}{H_i} < \alpha - \beta \tag{2.83}$$

where $F = h - d$ is the freeboard of the dam and where H_i is the incident (significant) wave height at the upwave side of the obstacle (dam), h is the crest level of the dam above the reference level (same as reference level of the bottom), d the mean water level relative to the reference level, and the coefficients α, β depend on the shape of the dam (Seelig, 1979) as given in Table 2.1. Expression (2.83) is based on experiments in a wave flume, so strictly speaking it is only valid for normal incidence waves. Since there are no data available on oblique waves, it is assumed that the transmission coefficient does not depend on direction. Another phenomenon that is to be expected is a change in wave frequency. Since often the process above the dam is highly nonlinear. Again there is little information available, so in SWAN it is assumed that the frequencies remain unchanged over an obstacle (only the energy scale of the spectrum is affected and not the spectral shape).

Table 2.1: Parameters for transmission according to Goda *et al.* (1967).

case	α	β
vertical thin wall	1.8	0.1
caisson	2.2	0.4
dam with slope 1:3/2	2.6	0.15

2.6 Wave-induced set-up

In a (geographic) 1D case the computation of the wave induced set-up is based on the vertically integrated momentum balance equation which is a balance between the wave force (gradient of the wave radiation stress normal to the coast) and the hydrostatic pressure gradient (note that the component parallel to the coast causes wave-induced currents but no set-up).

$$\frac{dS_{xx}}{dx} + \rho g H \frac{d\overline{\eta}}{dx} = 0 \tag{2.84}$$

where d is the total water depth (including the wave-induced set-up) and η is the mean surface elevation (including the wave-induced set-up) and

$$S_{xx} = \rho g \int [n \cos^2 \theta + n - \frac{1}{2}] E d\sigma d\theta \tag{2.85}$$

is the radiation stress tensor.

Observation and computations based on the vertically integrated momentum balance equation of Dingemans *et al.* (1987) show that the wave-induced currents are mainly driven by the divergence-free part of the wave forces whereas the set-up is mainly due to the rotation-free part of these forces. To compute the set-up in 2D, it would then be sufficient to consider the divergence of the momentum balance equation. If the divergence of the acceleration in the resulting equation is ignored, the result is:

$$\frac{\partial F_x}{\partial x} + \frac{\partial F_y}{\partial y} - \frac{\partial}{\partial x}(\rho g H \frac{\partial \overline{\eta}}{\partial x}) - \frac{\partial}{\partial y}(\rho g H \frac{\partial \overline{\eta}}{\partial y}) = 0 \tag{2.86}$$

2.7 Modelling of diffraction

To accommodate diffraction in SWAN simulations, a phase-decoupled refraction-diffraction approximation is suggested (Holthuijsen *et al.*, 2003). It is ex-

pressed in terms of the directional turning rate of the individual wave components in the 2D wave spectrum. The approximation is based on the mild-slope equation for refraction and diffraction, omitting phase information. It does therefore not permit coherent wave fields in the computational domain.

In a simplest case, we assume there are no currents. This means that $c_\sigma = 0$. Let denotes the propagation velocities in geographic and spectral spaces for the situation without diffraction as: $c_{x,0}$, $c_{y,0}$ and $c_{\theta,0}$. These are given by:

$$c_{x,0} = \frac{\partial \omega}{\partial k} \cos\theta \, , c_{y,0} = \frac{\partial \omega}{\partial k} \sin\theta \, , c_{\theta,0} = -\frac{1}{k} \frac{\partial \omega}{\partial h} \frac{\partial h}{\partial n} \tag{2.87}$$

where k is the wave number and n is perpendicular to the wave ray. We consider the following eikonal equation

$$K^2 = k^2(1 + \delta) \tag{2.88}$$

with δ denoting the diffraction parameter as given by:

$$\delta = \frac{\nabla(cc_g \nabla\sqrt{E})}{cc_g\sqrt{E}} \tag{2.89}$$

where $E(x, y)$ is the total energy of the wave field ($\sim H_s^2$). Due to diffraction, the propagation velocities are given by:

$$c_x = c_{x,0}\overline{\delta} \, , c_y = c_{y,0}\overline{\delta} \, , c_\theta = c_{\theta,0}\overline{\delta} - \frac{\partial \overline{\delta}}{\partial x} c_{y,0} + \frac{\partial \overline{\delta}}{\partial y} c_{x,0} \tag{2.90}$$

where

$$\overline{\delta} = \sqrt{1 + \delta} \tag{2.91}$$

In early computations, the wave fields often showed slight wiggles in geographic space with a wavelength of about $2\Delta x$ in $x-$direction. These unduly affected the estimations of the gradients that were needed to compute the diffraction parameter δ. The wave field was therefore smoothed with the following convolution filter:

$$E_{i,j}^n = E_{i,j}^{n-1} - 0.2[E_{i-1,j} + E_{i,j-1} - 4E_{i,j} + E_{i+1,j} + E_{i,j+1}]^{n-1} \tag{2.92}$$

where i, j is a grid point and the superscript n indicates iteration number of the convolution cycle. The width of this filter (standard deviation) in $x-$direction ε_x, when applied n times is

$$\varepsilon_x \approx \frac{1}{2}\sqrt{3n}\Delta x \tag{2.93}$$

By means of computations, $n = 6$ is found to be an optimum value (corresponding to spatial resolution of 1/5 to 1/10 of the wavelength), so that $\varepsilon_x \approx 2\Delta x$. For the $y-$direction, the expressions are identical, with y replacing x. Note that this smoothing is only applied to compute the diffraction parameter δ. For all other computations the wave field is not smoothed.

Chapter 3

Numerical approaches

3.1 Introduction

The accuracy with which physical processes for wave growth are approximated numerically is of crucial importance in assessing the predictive realism of spectral wave models. There is a need to separate these numerical errors from errors due to physical modelling. Third-generation wave models pose a numerical difficulty caused by the presence of multiple time scales. This is a reflection of the physical nature of wind waves, which consist of a wide range of frequencies. The ratio of the largest to the smallest time scale of spectral components is often substantially larger than one. When this is the case, the action balance equation is called stiff (Press *et al.*, 1993)[1]. Taking proper account of these time scales is a necessary condition for numerical accuracy. This would require the use of a very small time step in a numerical algorithm, which may be impractical. Moreover, the action balance equation is usually so stiff that its numerical implementation combined with economically large time steps often prevent a stable solution. In this respect, nonlinear four-wave interaction usually poses the biggest problem, since this process is associated with high sensitivity to spectral change.

In a number of papers concerning spectral wave computation, numerical measures are proposed to achieve stable model results economically. WAMDI Group (1988) suggest to use a semi-implicit time integration scheme with

[1]The equivalent situation for such an equation is to have eigenvalues of very different magnitudes.

a time step that matches the time scale of low-frequency waves. However, numerically stable solution of the resulting sytem of equations can not be guaranteed (Hargreaves and Annan, 2001). The ratio of the largest eigenvalue to the smallest eigenvalue of the stiff system of equations, called the condition number, can be so large that even a fully-implicit method combined with large time steps precludes a stable solution. For counterexamples, see Hargreaves and Annan (2001). The only remedy is time step reduction or under-relaxation so that the modified system of equations has a spectrum of eigenvalues with a more favourable condition number.

To guarantee numerical stability at relatively large time steps, the so-called action density limiter has been introduced in WAM in the early 1980's (Hersbach and Janssen, 1999). This limiter restricts the rate of change of the energy spectrum at each time step. Because low-frequency waves carry the most energy, it is desirable to solve the balance equation in this part of the spectrum accurately without intervention by the limiter, whereas for high-frequency waves using an equilibrium level is sufficient. Although this approach lacks a rigorous foundation and is not generally applicable or valid, it appears to guarantee numerical stability at relatively large time steps even when these do not match the time scales of wave growth. Moreover, it is believed that the limiter will not affect the stationary solution when convergence is reached. This assumption is widely employed as a justification for the use of limiters. For an overview, we refer to Hersbach and Janssen (1999) and Tolman (2002) and the references quoted therein. Tolman (1992) proposes an alternative to the action density limiter in which the time step is dynamically adjusted where necessary to ensure accurate wave evolution. The calculation of this optimal time step is related to the action density limiter. Further details can be found in Tolman (1992, 2002). .

The steady-state solution in the SWAN model is obtained in an iterative manner, which can be regarded as a time marching method with a pseudo time step. This pseudo time step generally does not match the relatively small time scale in frequency space and consequently, divergence will occur. Therefore, SWAN makes use of the action density limiter to stabilize the iteration process (Booij *et al.*, 1999). However, experience with SWAN has revealed that the limiter acts not only in the equilibrium space, but also in the energy-containing part of the wave spectrum. This finding is also confirmed by Tolman (2002). Furthermore, the limiter appears to be active over

almost all spectra in the geographical domain and during the entire iteration process. This activity has been associated with poor convergence behaviour, such as small-amplitude oscillation in frequency space. Ris (1999) demonstrated that stationary SWAN results are influenced by the settings of the action limiter while De Waal (2001) suspects that the limiter acts as a hidden sink in the source term balance under equilibrium conditions. The question to what extent this limiter adversely affects the stationary solution of SWAN has not been addressed previously, and is considered here.

An alternative way to restrict the high rate of change at higher frequencies is under-relaxation, i.e. making smaller updates by means of a much smaller (pseudo) time step (Ferziger and Perić, 1999). Consequently, a limiter may no longer be needed. Although this approach may be suitable to SWAN, it slows down convergence significantly. In this paper, we propose a new method that finds a compromise between fast convergence on the one hand and minimizing the role of the limiter in the energetic part of the spectrum on the other. The key idea to achieve this is to link the extent of updating to the wave frequency—the larger the frequency, the smaller the update. This approach is therefore called frequency-dependent under-relaxation.

The second objective of this paper concerns the formulation and the use of termination criteria required by the iteration procedure in SWAN. In principle, the iterative process should be stopped if the convergence error defined as the difference between the current iterate and the stationary solution is smaller than a prescribed tolerance. At present, the stopping criteria in SWAN make use of the difference between successive iterates as a measure of the error in the converged solution. Experiences in the application of SWAN have shown that the iteration process is often more erratic and typically much slower than reported by Booij *et al.* (1999). As a result, the current stopping criteria often lead to premature termination of simulations. This is characterised by the fact that, due to the relatively low rate of convergence, the convergence error is larger than the difference between the successive iterates. A stopping criterion is proposed that uses the second derivative or curvature of the series of successive iterates of the calculated wave height. The premise is that this curvature approaches zero upon full convergence.

3.2 Discretization

Discretization of (2.17) is carried out using the finite difference method. The homogeneous part of equation (2.17) is given by

$$\frac{\partial N}{\partial t} + \frac{\partial c_x N}{\partial x} + \frac{\partial c_y N}{\partial y} + \frac{\partial c_\sigma N}{\partial \sigma} + \frac{\partial c_\theta N}{\partial \theta}\,. \tag{3.1}$$

We choose a rectangular grid with constant mesh sizes Δx and Δy in $x-$ and $y-$direction, respectively. The spectral space is divided into elementary bins with a constant directional resolution $\Delta\theta$ and a constant relative frequency resolution $\Delta\sigma/\sigma$ (resulting in a logarithmic frequency distribution). We denote the grid counters as $1 \le i \le N_x$, $1 \le j \le N_y$, $1 \le l \le N_\sigma$ and $1 \le m \le N_\theta$ in $x-$, $y-$, $\sigma-$ and $\theta-$spaces, respectively. All variables are located at points (i, j, l, m). Time discretization takes place with the implicit Euler technique. We obtain the following approximation of (3.1):

$$\begin{aligned}\frac{N^n - N^{n-1}}{\Delta t}|_{i,j,l,m} \quad + \quad & \frac{[c_x N]_{i+1/2} - [c_x N]_{i-1/2}}{\Delta x}|^n_{j,l,m} + \\ & \frac{[c_y N]_{j+1/2} - [c_y N]_{j-1/2}}{\Delta y}|^n_{i,l,m} + \\ & \frac{[c_\sigma N]_{l+1/2} - [c_\sigma N]_{l-1/2}}{\Delta \sigma}|^n_{i,j,m} + \\ & \frac{[c_\theta N]_{m+1/2} - [c_\theta N]_{m-1/2}}{\Delta \theta}|^n_{i,j,l}\,,\end{aligned} \tag{3.2}$$

where n is a time-level with Δt a time step. Note that locations in between consecutive counters are reflected with the half-indices.

Since, the unknown N and the propagation velocities are only given in points (i, j, l, m), further approximation is needed. In the present paper, we employ a first order upwind scheme in geographical space, since it is sufficient accurate for nearshore applications and fully monotone, i.e. it can not to give rise to spurious oscillations. It should be noted, however, that in applications at oceanic scales, a higher order upwind scheme should be employed. In the current SWAN version, two alternatives to this scheme are implemented, namely the second order SORDUP and the third order Stelling/Leendertse schemes. See also Rogers *et al.* (2002) and Stelling and Leendertse (1992).

The fluxes $c_x N$ at $(i + 1/2, j, l, m)$ and $c_y N$ at $(i, j + 1/2, l, m)$ are approxi-

mated in the following way:

$$c_x N|_{i+1/2,j,l,m} = \begin{cases} c_x N|_{i,j,l,m}\,, & c_x|_{i,j,l,m} > 0 \\ c_x N|_{i+1,j,l,m}\,, & c_x|_{i+1,j,l,m} < 0 \end{cases} \tag{3.3}$$

and

$$c_y N|_{i,j+1/2,l,m} = \begin{cases} c_y N|_{i,j,l,m}\,, & c_y|_{i,j,l,m} > 0 \\ c_y N|_{i,j+1,l,m}\,, & c_y|_{i,j+1,l,m} < 0 \end{cases} . \tag{3.4}$$

The fluxes at $(i-1/2, j, l, m)$ and $(i, j-1/2, l, m)$ are obtained from (3.3) and (3.4), respectively, by decreasing the indices by 1 in appropriate manner. Note that the combination of the time and geographic space discretizations in (3.2), (3.3) and (3.4) is also known as the first order, backward space, backward time (BSBT) scheme.

SORDUP

For the SORDUP scheme which is the default scheme for stationary computations, the two terms in Eqs. (3.3) and (3.4) representing $x-$ and $y-$derivatives are replaced by

$$\left(\frac{1.5(c_x N)_{i_x} - 2(c_x N)_{i_x-1} + 0.5(c_x N)_{i_x-2}}{\Delta x} \right)^{i_t,n}_{i_y,i_\sigma,i_\theta} \tag{3.5}$$

and

$$\left(\frac{1.5(c_y N)_{i_y} - 2(c_y N)_{i_y-1} + 0.5(c_y N)_{i_y-2}}{\Delta y} \right)^{i_t,n}_{i_x,i_\sigma,i_\theta} \tag{3.6}$$

In the neighboorhood of open boundaries, land boundaries and obstacles (i.e., the last two grids adjoining such grid points for the SORDUP scheme), SWAN will revert to the first order upwind BSBT scheme. This scheme has a larger numerical diffusion but that is usually acceptable over the small distances involved.

Stelling and Leendertse scheme

For the Stelling and Leendertse scheme which is the default scheme for non-stationary computations, the two terms in Eqs. (3.3) and (3.4) representing $x-$ and $y-$derivatives are replaced by

$$\left(\frac{\frac{5}{6}(c_x N)_{i_x} - \frac{5}{4}(c_x N)_{i_x-1} + \frac{1}{2}(c_x N)_{i_x-2} \frac{1}{12}(c_x N)_{i_x-3}}{\Delta x} \right)^{i_t,n}_{i_y,i_\sigma,i_\theta} + \left(\frac{(c_x N)_{i_x+1} - (c_x N)_{i_x-1}}{4\Delta x} \right)^{i_t-1}_{i_y,i_\sigma,i_\theta} \tag{3.7}$$

and

$$\left(\frac{\frac{5}{6}(c_yN)_{i_y} - \frac{5}{4}(c_yN)_{i_y-1} + \frac{1}{2}(c_yN)_{i_y-2}\frac{1}{12}(c_yN)_{i_y-3}}{\Delta y}\right)^{i_t,n}_{i_x,i_\sigma,i_\theta} + \left(\frac{(c_yN)_{i_y+1} - (c_yN)_{i_y-1}}{4\Delta y}\right)^{i_t-1}_{i_x,i_\sigma,i_\theta} \tag{3.8}$$

In the neighboorhood of open boundaries, land boundaries and obstacles (i.e., the last three grids adjoining such grid points for the Stelling and Leendertse scheme), SWAN will revert to the first order upwind BSBT scheme.

Usually, the numerical diffusion of the Stelling and Leendertse scheme is so small that the so-called *garden-sprinkler effect* (GSE) may show up if propagation over very large distances is considered. This effect is due to the spectral resolution (see Booij and Holthuijsen (1987)). It can be counteracted by a diffusion term that has been explicitly added to the numerical scheme. Its value depends on the spectral resolution and the propagation time of the waves.

The diffusion applied in the propagation direction is

$$D_{ss} = \frac{\Delta c^2 T}{12} \tag{3.9}$$

where T is the wave age. The diffusion normal to the propagation direction is

$$D_{nn} = \frac{c^2 \Delta\theta^2 T}{12} \tag{3.10}$$

From these, diffusion coefficients are calculated as

$$D_{xx} = D_{ss}\cos^2\theta + D_{nn}\sin^2\theta\,, \quad D_{yy} = D_{ss}\sin^2\theta + D_{nn}\cos^2\theta\,, \quad D_{xy} = (D_{ss} - D_{nn})\cos\theta\sin\theta \tag{3.11}$$

The diffusion terms are computed at the time level $i_t - 1$. The diffusion terms are computed as follows

$$D_{xx}\left(\frac{(N)_{i_x+1} - 2(N)_{i_x} + (N)_{i_x-1}}{\Delta x^2}\right)^{i_t-1}_{i_y,i_\sigma,i_\theta} \tag{3.12}$$

$$D_{yy}\left(\frac{(N)_{i_y+1} - 2(N)_{i_y} + (N)_{i_y-1}}{\Delta y^2}\right)^{i_t-1}_{i_x,i_\sigma,i_\theta} \tag{3.13}$$

$$D_{xy}\left(\frac{(N)_{i_x,i_y} - (N)_{i_x-1,i_y} - (N)_{i_x-1,i_y} + (N)_{i_x-1,i_y-1}}{\Delta x\Delta y}\right)^{i_t-1}_{i_\sigma,i_\theta} \tag{3.14}$$

This explicit scheme is fast (having little impact on computation time) but only conditionally stable. Through mathematical analysis (not shown) it can be shown that a likely stability condition for the one-dimensional Stelling and Leendertse scheme with this GSE correction is $\Delta t/\Delta x^2 \leq 0.5$ which corresponds to the two-dimensional stability criterion of Tolman (1995) based on Fletcher (1988), Part I, section 7.1.1.:

$$Q = \frac{\max(D_{xx}, D_{yy}, D_{xy})\Delta t}{\min(\Delta x, \Delta y)^2} \leq 0.5 \tag{3.15}$$

Thus, it is credible that Eq. (3.15) holds true for the two-dimensional Stelling and Leendertse scheme with this GSE correction. In experiments, it was found that with $Q \leq 0.48$, no instability was observed. In short, by adding the GSE correction, the unconditionally stable advection scheme of SWAN becomes a (likely) conditionally stable advection-diffusion scheme. It is readily shown that for typical ocean applications D_{nn} dominates the diffusion and Q can be written as

$$Q = \frac{\overline{C}^2 T \Delta t}{12\Delta x^2} \tag{3.16}$$

The variable wave age $\overline{T}$ could be computed during the computations of SWAN but it requires the same order of magnitude of computer memory as integrating the action balance equation. Instead a constant wave age $\overline{T}$ can be used as an approximation, so that Eq. (3.16) becomes

$$Q = \frac{\overline{L}\mu\Delta\theta^2}{12\Delta x} \tag{3.17}$$

where the characteristic travel distance of the waves is $\overline{L} = \overline{CT}$ (e.g., the dimension of the ocean basin). For oceanic applications, the Courant number is typically $\mu \approx \frac{1}{2}$ so that $Q \leq 0.25$ for typical values of $\Delta\theta$ and $\overline{L}/\Delta x$ (the number of grid point in one direction of the grid). This implies that the Stelling and Leendertse scheme with the GSE correction is stable for typical ocean cases. For shelf sea (regional) applications, the value of $\mu = \mathcal{O}(1)$ but the garden-sprinkler effect tends to be small on these scales and the diffusion can and should not be used to avoid the stability problem. For small-scale (local) applications, typically $\mu = \mathcal{O}(10 - 100)$. But such cases are usually treated as stationary and the SORDUP scheme should be used (no GSE correction is included in this scheme).

The fluxes in the spectral space (σ, θ), as given in (3.2), should not be approximated with the first order upwind scheme since, it turns out to be very diffusive for frequencies near the blocking frequency[2]. Central differences should be used because of second order accuracy. However, such schemes tend to produce unphysical oscillations due to relatively large gradients in action density near the blocking frequency. Instead, a hybrid central/upwind scheme is employed:

$$c_\sigma N|_{i,j,l+1/2,m} = \begin{cases} (1-0.5\mu)c_\sigma N|_{i,j,l,m} + 0.5\mu c_\sigma N|_{i,j,l+1,m}\,, & c_\sigma|_{i,j,l,m} > 0 \\ \\ (1-0.5\mu)c_\sigma N|_{i,j,l+1,m} + 0.5\mu c_\sigma N|_{i,j,l,m}\,, & c_\sigma|_{i,j,l+1,m} < 0 \end{cases} \tag{3.18}$$

and

$$c_\theta N|_{i,j,l,m+1/2} = \begin{cases} (1-0.5\nu)c_\theta N|_{i,j,l,m} + 0.5\nu c_\theta N|_{i,j,l,m+1}\,, & c_\theta|_{i,j,l,m} > 0 \\ \\ (1-0.5\nu)c_\theta N|_{i,j,l,m+1} + 0.5\nu c_\theta N|_{i,j,l,m}\,, & c_\theta|_{i,j,l,m+1} < 0 \end{cases}, \tag{3.19}$$

where the parameters μ and ν are still to be chosen. For all values $\mu \in [0,1]$ and $\nu \in [0,1]$, a blended form arises between first order upwind differencing ($\mu = \nu = 0$) and central differencing ($\mu = \nu = 1$).

3.3 Solution algorithm

The discretization of the action balance equation (2.17) as described in Section 3.2 yields a system of linear equations that need to be solved. The corresponding matrix structure can take different forms, mainly depending on the propagation of wave energy in the geographic space. For instance, suppose that $c_x > 0$ and $c_y > 0$, everywhere. Then, the matrix structure has

[2]Waves can be blocked by the current at a relative high frequency.

the following form:

$$\left[\begin{array}{ccc}
\begin{pmatrix} .\,x\,.\,x\,x\,x\,.\,x\,.\,. \\ .\,.\,x\,.\,x\,x\,x\,.\,x\,. \\ .\,.\,.\,x\,.\,x\,x\,x\,.\,x \end{pmatrix} & & \\
\begin{pmatrix} .\,.\,.\,.\,x\,.\,.\,.\,.\,.\,.\,. \\ .\,.\,.\,.\,.\,.\,x\,.\,.\,.\,.\,. \\ .\,.\,.\,.\,.\,.\,.\,.\,x\,.\,.\,. \end{pmatrix} & \begin{pmatrix} .\,x\,.\,x\,x\,x\,.\,x\,.\,. \\ .\,.\,x\,.\,x\,x\,x\,.\,x\,. \\ .\,.\,.\,x\,.\,x\,x\,x\,.\,x \end{pmatrix} & \\
\begin{pmatrix} .\,.\,.\,.\,x\,.\,.\,.\,.\,.\,.\,. \\ .\,.\,.\,.\,.\,.\,x\,.\,.\,.\,.\,. \\ .\,.\,.\,.\,.\,.\,.\,.\,x\,.\,.\,. \end{pmatrix} & \begin{pmatrix} .\,.\,.\,.\,x\,.\,.\,.\,.\,.\,.\,. \\ .\,.\,.\,.\,.\,.\,x\,.\,.\,.\,.\,. \\ .\,.\,.\,.\,.\,.\,.\,.\,x\,.\,.\,. \end{pmatrix} & \begin{pmatrix} .\,x\,.\,x\,x\,x\,.\,x\,.\,. \\ .\,.\,x\,.\,x\,x\,x\,.\,x\,. \\ .\,.\,.\,x\,.\,x\,x\,x\,.\,x \end{pmatrix}
\end{array}\right]. \tag{3.20}$$

One recognizes that the subblocks on the main diagonal express coupling among the unknowns in the $(\sigma, \theta)-$space for each geographic grid point, whereas the off-diagonal subblocks represent coupling across geographical grid points. This system can be solved with a Gauss-Seidel technique in one step (Wesseling, 1992). Generally, the velocities c_x and c_y may have different signs in the geographical domain and hence, more steps are needed. However, it is well known that adapting the ordering of updates of the unknowns N in geographical space to the propagation direction can improve the rate of convergence of the Gauss-Seidel iterative procedure (Wesseling, 1992). This is done as follows. For each iteration, sweeping through grid rows and columns in geographical domain are carried out, starting from each of the four corners of the computational grid. After four sweeps, wave energy has been propagated over the entire geographical domain. During each sweep, only a subset of the unknown values of N are updated depending on the sign of c_x and c_y. For instance, the first sweep starts at the lower left-hand corner and all grid points with $c_x > 0$ and $c_y > 0$ are updated.

After each propagation update at geographic grid point, an update in the spectral space is made. Since, according to (3.3) and (3.4), the wave energy at a single spatial location depends on the upwind grid points only, it is sufficient to carry out the update within a 90^o-quadrant of the (σ, θ)-space, as illustrated in Figure 3.1. Because of the implicit nature of the spectral propagation terms in (3.2), a system of equations must be formed. Furthermore, due to the fact that the source term S_{tot} in (3.2) is nonlinear in N, linearization is required in order to find a solution. Generally, the term S_{tot}

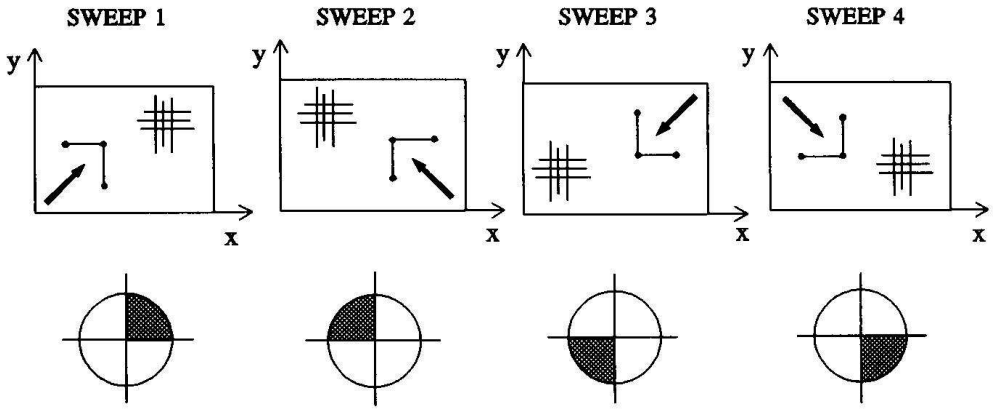

Figure 3.1: The solution procedure for wave energy propagation in geographical space with the appropriate directional quadrant (indicated by shaded area) for each of four sweeps.

in each bin (l, m) is treated by distinguishing between positive and negative contributions and arranging these in the linear form (Ferziger and Perić, 1999):

$$S_{\text{tot}} = S^p_{\text{tot}} + S^n_{\text{tot}} N \,, \tag{3.21}$$

where S^p_{tot} consists of positive contributions and S^n_{tot} of negative ones. Both contributions are independent of the solution N at the corresponding bin (l, m). Any negative term that does not contain N as a multiplier is first divided by N obtained from the previous iteration level and then added to S^n_{tot}. This stabilizes the iteration process. Details on the application of this principle to each source term in SWAN can be found in Booij *et al.* (1999).

The strongly nonlinear source term of depth-induced wave breaking is linearized by means of the Newton-Raphson iteration, as follows:

$$S^n \approx \phi^{n-1} E^n + \left(\frac{\partial S}{\partial E}\right)^{n-1} (E^n - E^{n-1}) \tag{3.22}$$

Since, this process of depth-induced wave breaking has been formulated such that $S = aS_{\text{tot}}$ and $E = aE_{\text{tot}}$, the derivative $\partial S/\partial E$ is analytically determined as $\partial S_{\text{tot}}/\partial E_{\text{tot}}$. Here, a is identical in both expressions and the total energy E_{tot} and total source S_{tot} are the integrals over all frequencies and

directions of $E(\sigma,\theta)$ and $S_{\mathrm{ds,br}}(\sigma,\theta)$, respectively.

As such, each difference equation (3.2) using expressions (3.18), (3.19) and (3.21) provides an algebraic relation between N at the corresponding bin and its nearest neighbours:

$$a_{\mathrm{P}}N_{\mathrm{P}} = a_{\mathrm{L}}N_{\mathrm{L}} + a_{\mathrm{R}}N_{\mathrm{R}} + a_{\mathrm{B}}N_{\mathrm{B}} + a_{\mathrm{T}}N_{\mathrm{T}} + b_{\mathrm{P}}\,, \tag{3.23}$$

where P corresponds to central bin (l,m) and L(eft), R(ight), B(ottom) and T(op) correspond to $(l-1,m)$, $(l+1,m)$, $(l,m-1)$ and $(l,m+1)$, respectively. Furthermore, the coefficients a_k, $k \in \{\mathrm{P},\mathrm{L},\mathrm{R},\mathrm{B},\mathrm{T}\}$ arise from the discretizations of the fluxes $c_\sigma N$ and $c_\theta N$ and b_{P} contains the positive contributions of the source term S^p_{tot} in (3.21) and the updated fluxes $c_x N$ (3.3) and $c_y N$ (3.4). Note that coefficient a_{P} includes $-S^n_{\mathrm{tot}}$.

The linear system of equations (3.23) for all bins within a directional quadrant at a particular geographical point is denoted by

$$A\,\vec{N} = \vec{b}\,, \tag{3.24}$$

where $A \in I\!R^{K\times K}$ contains the coefficients a_k, $k \in \{\mathrm{P},\mathrm{L},\mathrm{R},\mathrm{B},\mathrm{T}\}$ (and corresponds to a subblock on the main diagonal of (3.20)), $\vec{b} \in I\!R^K$ contains the coefficient b_{P} and boundary values and $\vec{N} \in I\!R^K$ denotes an algebraic vector containing the unknown action density values. Matrix A is non-symmetric. The dimension K of a directional quadrant equals $N_\sigma \times 1/4 N_\theta$. Note that linearization of the source term (3.21) enhances diagonal dominance of A, thereby improving numerical stability. Also note that neither A nor $\vec{b}$ depends on the unknowns. Each row in the matrix A corresponds to a bin (l,m). The main diagonal contains the coefficients a_{P} and directly to the left and right are the coefficients $-a_{\mathrm{B}}$ and $-a_{\mathrm{T}}$, respectively. The coefficients $-a_{\mathrm{L}}$ and $-a_{\mathrm{R}}$ are on the diagonals that are N_θ positions to the left and right of the main diagonal, respectively.

The solution $\vec{N}$ is given by $A^{-1}\vec{b}$. Since, the only non-zero matrix elements are situated in five diagonals, iterative solution methods that utilize the sparsity of A optimally are very attractive. In SWAN, the solution of (3.24) is found by means of an incomplete lower-upper decomposition method followed by an iteration process called the Strongly Implicit Procedure (SIP) (Ferziger and Perić, 1999). This procedure is specifically designed for (non-symmetric) penta-diagonal systems and is relatively fast. Note that in the

absence of mean current there are no shifts in the frequency, and consequently the structure of A reduces to a tri-diagonal one, i.e. $a_{\rm L} = a_{\rm R} = 0$, which can be inverted efficiently with the Thomas algorithm (Press *et al.*, 1993; Ferziger and Perić, 1999).

Due to refraction and nonlinear wave energy transfer, interactions occur between the directional quadrants. To properly take these interactions into account and the fact that we employ the Gauss-Seidel technique and linearization of the source term (3.21), the quadrant sweeping and the solution of system (3.24) need to be repeated until some convergence criteria are met. At present, the iteration process runs from $s = 1$ to $s = S$ and is terminated if the maximum number of iterations S (usually 15) is reached or the following criteria for the significant wave height H_{m0} and mean relative wave period T_{m01}, as given by

$$H_{m0} = 4\sqrt{m_0}\,, \quad T_{m01} = 2\pi\frac{m_0}{m_1}\,, \quad m_j = \int_0^{\infty}\int_0^{2\pi} \sigma^j E(\sigma,\theta) d\sigma d\theta\,, \qquad (3.25)$$

are both satisfied in at least 98% of all wet grid points (i, j):

$$\frac{|\Delta H^s_{m0}(i,j)|}{H^{s-1}_{m0}(i,j)} < \varepsilon^{\rm r}_{\rm H} \quad \text{or} \quad |\Delta H^s_{m0}(i,j)| < \varepsilon^{\rm a}_{\rm H} \qquad (3.26)$$

and

$$\frac{|\Delta T^s_{m01}(i,j)|}{T^{s-1}_{m01}(i,j)} < \varepsilon^{\rm r}_{\rm T} \quad \text{or} \quad |\Delta T^s_{m01}(i,j)| < \varepsilon^{\rm a}_{\rm T}\,. \qquad (3.27)$$

Here, $\Delta Q^s \equiv Q^s - Q^{s-1}$, with Q some quantity. In this study, we use the default values: $\varepsilon^{\rm r}_{\rm H} = \varepsilon^{\rm r}_{\rm T} = 0.02$, $\varepsilon^{\rm a}_{\rm H} = 0.02$ m and $\varepsilon^{\rm a}_{\rm T} = 0.2$ s; see Holthuijsen *et al.* (2003). The rationale behind the use of the integral wave parameters H_{m0} and T_{m01} in the stopping criteria is that these are the output variables typically of interest. The iterative solution procedure is accelerated by calculating a reasonable first guess of the wave field based on second-generation source terms of Holthuijsen and De Boer (1988).

3.4 Convergence-enhancing measures

As explained in Section 3.1, many time scales are involved in the evolution of wind waves. The high-frequency waves have much shorter time scales than the low-frequency waves, rendering the system of equations (3.24) stiff. If no

special measures are taken, the need to resolve high-frequency waves at very short time scales would result in extreme computational time. For economy, it is desirable that a numerical technique can be used with a large, fixed time step. Moreover, we are mainly interested in the evolution of slowly changing low-frequency waves. For stationary problems, we are interested in obtaining the steady-state solution. Unfortunately, the convergence to the steady state is dominated by the smallest time scale and, in the absence of remedial measures, destabilizing over- and undershoots will prevent solution from converging monotonically during the iteration process. These oscillations arise because of the off-diagonal terms in matrix A, which can be dominant over the main diagonal, particularly when the ratio $\sigma_{\max}/\sigma_{\min}$ is substantially larger than one. As a consequence, convergence is slowed down and divergence often occurs. To accelerate the iteration process without generating instabilities, appropriately small updates must be made to the level of action density.

With the development of the WAM model, a so-called action density limiter was introduced as a remedy to the abovementioned problem. This action limiter restricts the net growth or decay of action density to a maximum change at each geographic grid point and spectral bin per time step. This maximum change corresponds to a fraction of the omni-directional Phillips equilibrium level (Hersbach and Janssen, 1999). In the context of SWAN (Booij *et al.*, 1999), this is

$$\Delta N \equiv \gamma \frac{\alpha_{\mathrm{PM}}}{2\sigma k^3 c_g}\,, \tag{3.28}$$

where $\gamma \geq 0$ denotes the limitation factor, k is the wave number and $\alpha_{\mathrm{PM}} = 8.1\times10^{-3}$ is the Phillips constant for a Pierson-Moskowitz spectrum (Komen *et al.*, 1994). Usually, $\gamma = 0.1$ (Tolman, 1992)[3]. Denoting the total change in $N_{i,j,l,m}$ from one iteration to the next after (3.2) by $\Delta N_{i,j,l,m}$, the action density at the new iteration level is given by

$$N^s_{i,j,l,m} = N^{s-1}_{i,j,l,m} + \frac{\Delta N_{i,j,l,m}}{|\Delta N_{i,j,l,m}|}\,\min\{|\Delta N_{i,j,l,m}|, \Delta N\}\,. \tag{3.29}$$

For wave components at relatively low frequencies, (3.29) yields the pre-limitation outcome of (3.2), because, for these components, the pseudo time

[3]It is noted here that the effective γ used in SWAN is not equivalent to that of WAM: the former is a factor 2π larger.

step matches the time scale of their evolution. For high-frequency waves, however, (3.29) gives the upper limit for the spectrum to change per iteration due to the limiter (3.28). For typical coastal engineering applications, it is sufficient to compute the energy-containing part of the wave spectrum accurately. In other words, action densities near and below the spectral peak should not be imposed by the limiter (3.28). However, our experiences with SWAN have shown that the limiter is active even close to the peak. Furthermore, during the entire iteration process, the limiter is typically active at almost every geographic grid point.

The alternative measure to enhance the convergence of the stable iteration process considered here is so-called false time stepping (Ferziger and Perić, 1999). Under-relaxation terms representing the rate of change are introduced to enhance the main diagonal of A and thus stabilize the iteration process. The system of equations (3.24) is replaced by the following, iteration-dependent system

$$\frac{\vec{N}^s - \vec{N}^{s-1}}{\tau} + A\,\vec{N}^s = \vec{b} \tag{3.30}$$

with τ a pseudo time step. The first term of (3.30) controls the rate of convergence of the iteration process in the sense that smaller updates are made due to decreasing τ, usually at the cost of increased computational time. To deal with decreasing time scales at increasing wave frequency, the amount of under-relaxation is enlarged in proportion to frequency. This allows a decrease in the computational cost of under-relaxation, because at lower frequencies larger updates are made. This frequency-dependent under-relaxation can be achieved by setting $\tau^{-1} = \alpha\sigma$, where α is a dimensionless parameter. The parameter α will play an important role in determining the convergence rate and stability of the iteration process. Substitution in (3.30) gives

$$(A + \alpha\sigma I)\,\vec{N}^s = \vec{b} + \alpha\sigma\vec{N}^{s-1}\,. \tag{3.31}$$

When the steady state is reached (i.e. $s \to \infty$), system (3.31) solves $A\,\vec{N}^\infty = \vec{b}$ since, $\vec{N}^\infty$ is a fixed point of (3.31).

Suitable values for α must be determined empirically and thus robustness is impaired. For increasing values of α, the change in action density per iteration will decrease in the whole spectrum. The consequence of this is twofold. Firstly, it allows a much broader frequency range in which the action balance

equation (3.2) is actually solved without distorting convergence properties. Secondly, the use of the limiter will be reduced because more density changes will not exceed the maximum change (3.28). Clearly, this effect may be augmented by increasing the value of γ in (3.28).

To allow proper calculation of the second-generation first guess of the wave field (see Section 3.3), under-relaxation is temporarily disabled ($\alpha = 0$) during the first iteration. Whereas this measure is important in achieving fast convergence, it does not affect stability, since the second-generation formulations do not require stabilization.

3.5 Stopping criteria

In general, the iterative method should be stopped if the approximate solution is accurate enough. A good termination criterion is very important, because if the criterion is too weak the solution obtained may be useless, whereas if the criterion is too severe the iteration process may never stop or may cost too much work. Experiences with SWAN have shown that the present criteria (3.26) and (3.27) are often not strict enough to obtain accurate results after termination of the iterative procedure. Thus, criteria (3.26) and (3.27) are necessary but not sufficient. It was found that the iteration process can converge so slowly that at a certain iteration s the difference between the successive iterates, $H_{m0}^s - H_{m0}^{s-1}$, can be small enough to meet the convergence criteria, causing the iteration process to stop, even though the converged solution has not yet been found. In particular, this happens when convergence is non-monotonic such that the process is terminated at local maxima or minima that may not coincide with the converged solution.

Furthermore, it became apparent that, unlike H_{m0}, the quantity T_{m01} is not an effective measure of convergence. It was found that the relative error in T_{m01}, i.e. $|T_{m01}^s - T_{m01}^{s-1}|/T_{m01}^{s-1}$, does not monotonically decrease near convergence, but keeps oscillating during the iteration process. This behaviour is due to small variations in the spectrum at high frequencies, to which T_{m01} is sensitive. This behaviour is problematic when any form of stricter stopping criterion is developed based on T_{m01}. Therefore, in the improved termination criterion proposed in this paper, T_{m01} has been abandoned as a convergence measure and only H_{m0}, which displays more monotonic behaviour near convergence, is retained.

Stiffness and nonlinearity of the action balance equation are found to yield less rapid and less monotone convergence. Ferziger and Perić (1999) explain the slow convergence in terms of the eigenvalue or spectral radius of the iteration process generating the sequence $\{\phi^0, \phi^1, \phi^2, ...\}$. They show that the actual solution error is given by

$$\phi^{\infty} - \phi^s \approx \frac{\phi^{s+1} - \phi^s}{1 - \rho}\,, \tag{3.32}$$

where ϕ^{∞} denotes the steady-state solution and ρ is the spectral radius indicating the rate of convergence. The smaller ρ, the faster convergence. This result shows that the solution error is larger than the difference between successive iterates. Furthermore, the closer ρ is to 1, the larger the ratio of solution error to the difference between successive iterates. In other words, the lower the rate of convergence of the iteration process, the smaller this difference from one iteration to the next must be to guarantee convergence. The stopping criterion of SWAN could be improved by making the maximum allowable relative increment in H_{m0} a function of its spectral radius instead of imposing a fixed allowable increment. By decreasing the allowable relative increment as convergence is neared, it would be possible to delay run termination until a more advanced stage of convergence. Such a stopping criterion was used by, e.g. Zijlema and Wesseling (1998). This criterion is adequate if the iteration process converges in a well-behaved manner and $\rho < 1$ for all iterations. However, due to nonlinearities SWAN typically does not display such smooth behaviour. Therefore, this criterion may be less suited for SWAN.

An alternative way to evaluate the level of convergence is to consider the second derivative or curvature of the curve traced by the series of iterates (iteration curve). Since the curvature of the iteration curve must tend towards zero as convergence is reached, terminating the iteration process when a certain minimum curvature has been reached would be a robust break-off procedure. The curvature of the iteration curve of H_{m0} may be expressed in the discrete sense as

$$\Delta(\Delta\tilde{H}^s_{m0})^s = \tilde{H}^s_{m0} - 2\tilde{H}^{s-1}_{m0} + \tilde{H}^{s-2}_{m0}\,, \tag{3.33}$$

where $\tilde{H}^s_{m0}$ is some measure of the significant wave height at iteration level s. To eliminate the effect of small amplitude oscillations on the curvature mea-

sure, we define $\tilde{H}^s_{m0} \equiv (H^s_{m0} + H^{s-1}_{m0})/2$. The resulting curvature-based termination criterion at grid point (i, j) is then

$$\frac{|H^s_{m0}(i,j) - (H^{s-1}_{m0}(i,j) + H^{s-2}_{m0}(i,j)) + H^{s-3}_{m0}(i,j)|}{2H^s_{m0}(i,j)} < \varepsilon_{\mathrm{C}}\,, \quad s = 3, 4, \ldots\,, \tag{3.34}$$

where ε_{C} is a given maximum allowable curvature. The curvature measure is made non-dimensional through normalization with H^s_{m0}. Condition (3.34) must be satisfied in at least 98% of all wet grid points before the iterative process stops. This curvature requirement is considered to be the primary criterion. However, the curvature passes through zero between local maxima and minima and, at convergence, the solution may oscillate between two constant levels due to the action limiter, whereas the average curvature is zero. As safeguard against such a situation, the weaker criterion (3.26) is retained in addition to the stricter criterion (3.34).

Chapter 4

Wave boundary and initial conditions

To obtain the numerical solution of the action balance equation (2.16), the wave boundary and initial conditions should be provided. The incoming wave components at the up-wave boundaries in the SWAN model are specified by a two-dimensional spectrum. Several options are available:

- A parametric one-dimensional spectrum with a certain imposed directional distribution. An example is a Jonswap spectrum.
- A discrete one-dimensional spectrum with a certain imposed directional distribution. This is often obtained from measurements.
- A discret two-dimensional spectrum. This may be obtained from other SWAN runs or other models, e.g. WAM and WAVEWATCH III.

For the parametric one-dimensional spectrum, the following optional forms have been recommended: a Pierson-Moskowitz spectrum (Pierson and Moskowitz, 1964), a Jonswap spectrum (Hasselmann *et al.*, 1973) and a Gaussian-shaped spectrum.

The boundaries in frequency space are fully absorbing at the lowest and the highest discrete frequency. So, energy can freely propagate across these boundaries and thus total energy might not be conserved in some cases. However, a diagnostic tail f^{-m} ($m = 4$ or $m = 5$) is added above the high frequency cut-off, which is used to compute nonlinear wave-wave interactions at the high frequencies and to compute integral wave parameters. When the

directional space is a closed circular, no directional boundary conditions are needed. However, for reasons of economy, SWAN has an option to compute only wave components in a pre-defined directional sector. In this case, the boundaries of this sector are fully absorbing (action density might be removed from the model by refraction).

To facilitate the integration process of the action balance equation, wave boundary conditions in geographical space need to be provided. The boundaries of the computational grid in SWAN are either land or water. In case of land there is no problem. The land does not generate waves and in SWAN it absorbs all incoming wave energy. But in the case of a water boundary there is a problem. If observations are available, they can be used as inputs at the boundary. In case no wave conditions are given along the boundary, SWAN assumes that no waves enter the model and waves can leave the model freely along that boundary. This assumption results in errors. Therefore, to get reliable results, especially for such case, the model boundaries must be placed far away from the area of interest.

In case of non-stationary computation, the default initial spectra are computed from the local wind velocities using the deep-water growth curve of Kahma and Calkoen (1992), cut off at values of significant wave height and peak frequency from Pierson and Moskowitz (1964). The average (over the model area) spatial step size is used as fetch with local wind. The shape of the spectrum is default Jonswap with a $\cos^2(\theta)$ directional distribution centred around the local wind direction.

The first guess conditions of a stationary run of SWAN are default determined with the second generation mode of SWAN.

It is possible to obtain an initial state by carrying out a previous stationary or nonstationary computation.

Chapter 5

Implementation of 2D wave set-up

5.1 Methods

For the present purpose flows in shallow water are sufficiently described by the so- called shallow-water equation which consists of one continuity equation and two equations of motion (one for the $x-$ and one for the $y-$component). For the present project the shallow water equation has to be simplified. The possibilities for such simplification are investigated in the remainder of this section.

Wave setup is usually confined to narrow zones in the immediate vicinity of the shoreline. The size of such areas is small enough that the setup process can be considered to be quasi-stationary.

Wave-induced currents are usually weak compared with e.g. tidal currents. Therefore it seems acceptable to neglect all terms in the equation of motion where the current velocity appears.

Comparisons of SWAN results with results from a full 2-dimensional flow model have to show under which conditions the simplified equation provides acceptable results. Such investigations are outside the scope of the present project. This report presents a few cases with low overall current velocities where apparently the computed setup is reasonably in accordance with expectations.

Deleting from the equation of motion all terms involving current velocities we retain an equilibrium between the wave-induced force and the gradient of the water table, i.e.

$$F_k + gd\frac{\partial \zeta}{\partial x_k} = 0 \ , \tag{5.1}$$

where ζ is the setup, d the depth and F_k is the wave-induced force. In a one-dimensional model (5.1) can be used directly to compute the setup. In two dimensions (5.1) is a set of two equations with only one unknown, the setup ζ. In order to reduce the number of equations to one, we use the observation by Dingemans(1997) that wave-driven currents are mainly due to the divergence-free part of the wave forces whereas the setup is mainly due to the rotation-free part of the force field. We therefore take the divergence of eq. (5.1) to obtain the following elliptic partial differential equation for ζ:

$$\frac{\partial F_k}{\partial x_k} + \frac{\partial}{\partial x_k}(gd\frac{\partial \zeta}{\partial x_k}) = 0 \tag{5.2}$$

This Poisson equation needs one boundary condition in each point of the boundary of the computational domain. Two types of boundary conditions are foreseen; the first one is used on the open boundaries and on the shoreline where the shoreline is defined as the line where the depth is zero:

$$F_n + gd\frac{\partial \zeta}{\partial n} = 0 \tag{5.3}$$

It is not possible to use this boundary condition on all boundary points because then there remains an unknown constant. So on on point, for which we take the boundary point with the largest depth the setup is assumed to be 0: $\zeta = 0$.

The second type of boundary condition with given value of ζ is also used in nested models. The setup computed in the larger model is used as boundary condition in the nested model. In the nested model the setup is given in all points of the outer boundary. On shorelines inside the area again eq. (5.3) is used.

The Poisson equation (5.2) together with its boundary conditions will be solved numerically on a curvilinear grid. The next section dsicusses the details of the method, and presents some results of preliminary computations with the above model.

The actual design of the modifications of the SWAN commands is presented in Appendix A, the design of the modifications of the code is presented in Appendix B. After each iteration performed in SWAN new values of the setup are being calculated and added to the depth, so that the SWAN model incorporates the effect of setup on the wave field. An output quantity SETUP is added so that the user can be informed about the magnitude and distribution of the wave setup.

5.2 Analysis and Results

5.2.1 Discretization of the 2D setup equation

Problem definition

The equation to be solved has the following form:

$$\frac{\partial}{\partial x_k}(F_k + gd\frac{\partial \zeta}{\partial x_k}) = 0 \,, \tag{5.4}$$

with ζ the setup, d the depth and F_k a golf-induced, time-averaged force.
In order to solve (5.4), the following types of boundary conditions may be applied

$$F_n + gd\frac{\partial \zeta}{\partial n} = 0 \quad \text{at the boundary} \,, \tag{5.5}$$

with n the outward direct normal. This is a so-called Neumann condition. The setup is fixed upon an additive constant.

$$\zeta = \text{ given at the boundary} \,. \tag{5.6}$$

This is boundary condition of Dirichlet type.

At beaches always the Neumann condition (5.5) is applied.
In order to solve (5.4) with boundary conditions (5.5) and (5.6) a boundary fitted, vertex centered finite volume method is applied. The discretization is based on the method described in Van Beek *et al.* (1995). In the remainder of this Chapter we use k instead of gd.

Discretization

The physical domain is mapped onto a rectangular domain in the (ξ^1, ξ^2) plane, which is called the computational domain. All points of the domain are used, including the dry ones.

Using the relation Zijlema (1996) (summation convection applied):

$$\frac{\partial \varphi}{\partial x^\beta} = \frac{1}{\sqrt{g}} \frac{\partial}{\partial \xi^\gamma} (\sqrt{g}\ a_\beta^{(\gamma)}\ \varphi)\ , \tag{5.7}$$

with $a_\beta^{(\gamma)}$ the components of the contravariant basevectors $\vec{a}^{(\alpha)}$ defined as (Segal *et al*, 1992):

$$\vec{a}^{(\alpha)} = \nabla \xi^\alpha\ , \tag{5.8}$$

and $\sqrt{g}$ the Jacobian of the transformation:

$$\sqrt{g} = a^1_{(1)} a^2_{(2)} - a^2_{(1)} a^1_{(2)}\ . \tag{5.9}$$

$\vec{a}_{(\alpha)}$ are the covariant base vectors defined by

$$\vec{a}_{(\alpha)} = \frac{\partial \vec{x}}{\partial \xi^\alpha}\ . \tag{5.10}$$

The contravariant base vectors follow immediately from the covariant ones due to:

$$\sqrt{g}\vec{a}^{(1)} = (a^2_{(2)},\ -a^1_{(2)})^T\ , \tag{5.11}$$

$$\sqrt{g}\vec{a}^{(2)} = (-a^2_{(1)},\ a^1_{(1)})^T\ . \tag{5.12}$$

Application of (5.7) to equation (5.5) results in

$$\frac{1}{\sqrt{g}} \frac{\partial}{\partial \xi^\alpha} (\sqrt{g}\vec{a}^{(\alpha)} \cdot (k\nabla\zeta + \vec{F})) = 0\ . \tag{5.13}$$

Note that $\nabla\zeta$ is a derivative in the Cartesian $(\vec{x})$ direction and not in the $\vec{\xi}$ direction.

In the remainder we shall use the local numbering as given in Figure 5.1. The points (0, 0), (2, 0), (0, 2) and so on are the vertices of the cells. The integration cell for the finite volume method is defined by the cell Ω (-1, 0),

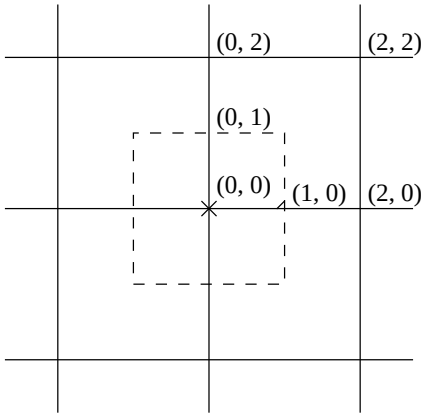

Figure 5.1: Local numbering in computational domain

(0, -1), (1, 0), (0, 1).

Integrating (5.13) over this cell gives

$$\begin{aligned}
&\int_{\Omega_x} \frac{1}{\sqrt{g}} \frac{\partial}{\partial \xi^\alpha} (\sqrt{g}\vec{a}^{(\alpha)} \cdot (k\nabla\zeta + \vec{F})) d\Omega_x \\
&\int_{\Omega_\xi} \frac{\partial}{\partial \xi^\alpha} (\sqrt{g}\vec{a}^{(\alpha)} \cdot (k\nabla\zeta + \vec{F})) d\Omega_\xi \qquad (5.14) \\
&\approx \sqrt{g}\vec{a}^{(1)} \cdot (k\nabla\zeta + F)|_{(-1,0)}^{(1,0)} + \sqrt{g}\vec{a}^{(2)} \cdot (k\nabla\zeta + \vec{F})|_{(0,-1)}^{(0,1)} ,
\end{aligned}$$

where Ω_x is the cell in the physical space and Ω_ξ the cell in the computational domain.
The four points (1, 0), (0, 1), (-1,0) and (0, -1) will be cell integration points. The covariant basis vectors $\vec{a}_{(\alpha)}$ are approximated by central differences.

$$\vec{a}_{(2)}|_{(0,1)} = \vec{x}_{(0,2)} - \vec{x}_{(0,0)} , \qquad (5.15)$$

$$\vec{a}_{(1)}|_{(1,0)} = \vec{x}_{(2,0)} - \vec{x}_{(0,0)} , \qquad (5.16)$$

and by linear interpolation in other points.
In these relations we have used that the step width in the computational domain is equal to 1.
The term $\nabla\zeta$ needs special attention. Since it concerns derivatives in the $\vec{x}$ direction, whereas all derivatives in the computational domain are in the $\vec{\xi}$ directions it is necessary to make some approximation. We approximate this

term by the integration path method introduced in Van Beek *et al.* (1995).

To that end $\nabla\zeta$ is integrated in two independent directions ξ^1 and ξ^2. This yields two equations to express $\frac{\partial\zeta}{\partial x}$ and $\frac{\partial\zeta}{\partial y}$ in ζ values of neighbours.

$$(\vec{x}_{2,0} - \vec{x}_{),0})\nabla\zeta|_{(1,0)} = \zeta_{2,0} - \zeta_{0,0} \ , \tag{5.17}$$

$$\frac{1}{2}((\vec{x}_{2,2} - \vec{x}_{2,-2}) + (\vec{x}_{0,2} - \vec{x}_{0,-2}))\nabla\zeta|_{(1,0)} = \frac{1}{2}((\zeta_{2,2} - \zeta_{2,-2}) + (\zeta_{0,2} - \zeta_{0,-2})) \tag{5.18}$$

(5.17), (5.18) may be considered as two sets of equations to express $\nabla\zeta$ into ζ values. Solution of this linear system results in:

$$\nabla\zeta|_{(1,0)} = \zeta|^{(2,0)}_{(0,0)}\vec{c}^{(1)} + (\zeta|^{(0,2)}_{(0,-2)} + \zeta|^{(2,2)}_{(2,-2)})\vec{c}^{(2)} \ , \tag{5.19}$$

with

$$\vec{c}^{1} = \frac{1}{C}(c^2_{(2)},\ -c^1_{(2)}) \ ; \ \vec{c}^{2} = \frac{1}{C}(-c^2_{(1)},\ c^1_{(1)}) \ , \tag{5.20}$$

$$C = c^2_{(2)}c^1_{(1)} - c^2_{(1)}c^1_{(2)} \ , \tag{5.21}$$

$$\vec{c}_{(1)} = a_{(1)}|_{(1,0)} \ \ \vec{c}_{(2)} = \vec{a}_{(2)}|_{(0,-1)} + \vec{a}_{(2)}|_{(0,1)} + \vec{a}_{(2)}|_{(2,-1)} + \vec{a}_{(2)}|_{(2,1)} \tag{5.22}$$

A similar formula is applied for point (0, 1). Equation (5.14) together with expression (5.19) gives one row of the discretized equation.

Treatment of the boundary conditions

The boundary conditions at the outer boundary of the domain are relatively easy to implement.

In case of Dirichlet boundary conditions the corresponding row of the matrix is made equal to 0 and the diagonal element is set to 1. The value of the boundary condition is filled into the right-hand side.

Neumann boundary conditions are treated integrating over a half cell as sketched in Figure 5.2. In this case we get:

$$\int_{\Omega_\xi} \frac{\partial}{\partial\xi^\alpha}(\sqrt{g}\vec{a}^{(\alpha)} \cdot (k\nabla\zeta + \vec{F})d\Omega_\xi$$

$$\simeq \frac{1}{2}\sqrt{g}\vec{a}^{(1)} \cdot (k\nabla\zeta + \vec{F})|^{(1,0)}_{(-1,0)} + \sqrt{g}\vec{a}^{(2)} \cdot (k\nabla\zeta + \vec{F})|^{(0,1)}_{(0,0)} \ . \tag{5.23}$$

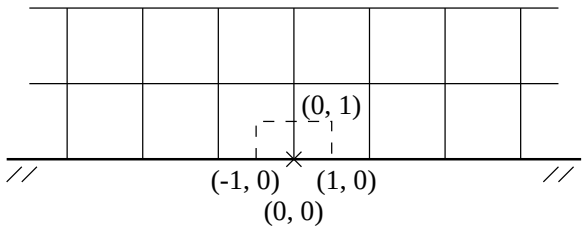

Figure 5.2: Half cell at boundary

Due to the Neumann boundary conditions the term in the boundary point (0, 0) vanishes.

Mark that in this case we need to evaluate $\nabla\zeta$ at the boundary. In order to do so we apply a one-sided integration path approach i.e.

$$(\vec{x}_{(2,0)} - \vec{x}_{(1,0)}) \cdot \nabla\zeta|_{(1,0)} = \zeta_{(2,0)} - \zeta_{(0,0)} \ ,$$
$$((x_{(2,2)} - x_{(2,0)}) + (\vec{x}_{(0,2)} - \vec{x}_{(0,0)})) \cdot \nabla\zeta|_{(1,0)} = (\zeta_{(0,2)} - \zeta_{(0,0)}) + (\zeta_{(2,2)} - \zeta_{(2,0)}) \quad (5.24)$$

Furthermore we need the values of $\vec{a}_{(\alpha)}$ in virtual cells, because we need the $c^{(\alpha)}$ at the boundary. To that end we construct a row of virtual cells by extrapolating the coordinates of the boundary cells.

The implementation of dry points

Dry points complicate the software considerably.

For the dry points itself there is no problem. In fact we make the corresponding row of the matrix, as well as the right-hand side element completely equal to zero. This is allowed since our linear solver is able to deal with zero rows.

Dry points in the neighbourhood of wet points, however, also influence the matrix for the wet point. Consider for example the integration point (1,0) in Figure 5.3. If (0, 0) is a wet point and (2, 0) a dry point then we assume that at point (1,0) we have a Neumann boundary condition. This means in fact that the contribution of the integration point (1,0) to the matrix and right-hand side is equal to zero. With respect to the evaluation of the gradient of ζ with the integration path method one sided differences are applied for those formulas involving $\zeta_{(2,0)}$. This process is applied for all transitions from wet to dry points. As a consequence, in the case of a situation like

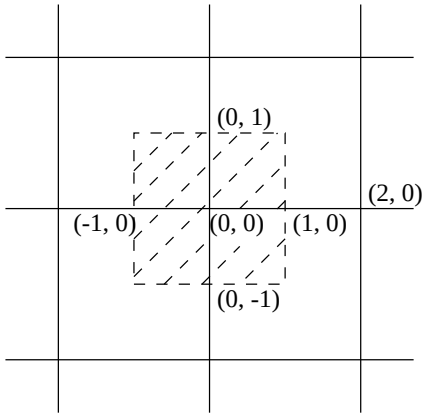

Figure 5.3: Dry point (2, 0) and wet point (0, 0)

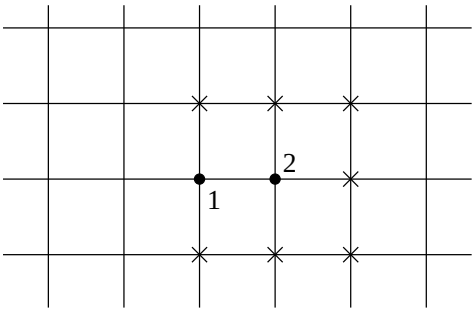

Figure 5.4: Wet points • enclosed by a row of dry points ×

in Figure 5.4 we make $\nabla\zeta$ for point 2 zero. The reason is that in point 2 it is only possible to evaluate $\frac{\partial\zeta}{\partial\xi^1}$ and not $\frac{\partial\zeta}{\partial\xi^2}$, and hence we have too few information to express $\nabla\zeta$ in neighbour values.

Building of the matrix and right-hand side

With respect to the building of matrix and right-hand side we start by computing all contributions in the integration points. This is done by looping over the various integration points. Since the contribution of point (0,1) in cell (i, j) is equal to that of point (0, -1) in cell $(i - 1, j)$ it is sufficient to loop over two sets of integration points only.

Once we have computed the coefficients in a set of integration points we must

add these contributions, multiplied by some factor, to the matrix elements. This process is known as distribution.

Hence the actual implementation is as follows:

1 Map indirect addressing to direct addressing. (subroutine swdct).

2 Compute and store $\vec{a}_{(\alpha)}$ for all integration points. First we use central differences where possible and after that we apply linear interpolation for the remaining points. (subroutine swcova2d).

3 Compute $\sqrt{g}\vec{a}^{(\alpha)}$ in all integration points using $\vec{a}_{(\alpha)}$. (subroutine swjcta2d).

For 2 integration directions do

4 Compute factors $\vec{c}^{(\alpha)}$ taking into account boundary effects and dry points.
Compute contributions for matrix and right-hand side for integration points.
(subroutine swtrad2d).

5 Distribute contribution to correct matrix elements.
(subroutine swdisdt2).

6 Fill essential boundary conditions.
(subroutine swessbc).

7 Solve system of linear equations.
(subroutine swsolve).
This part is explained in more detail in the next Chapter.

8 Map from direct to indirect addressing.
(subroutine swindct).

5.2.2 The iterative solver for the linear system

In this section we describe the mathematical methods, which are used to solve the system of linear equations as derived in Chapter 1. In Section 5.2.2 we consider the data structure used. Some properties of the matrix are given in Section 5.2.2. Due to the sparseness of the matrix we prefer an iterative solution method of Krylov subspace type. The details are described in Section

5.2.2. As is well known, Krylov subspace methods are only attractive when they are combined with suitable preconditioners (see Section **??**). Finally our choices are summarised in Section **??**.

Data structure

After the discretization of the Poisson equation in curvilinear coordinates, one has to solve the following matrix vector system:

$$Ax = f, \tag{5.25}$$

where A is the discrete Poisson operator, x is an approximation of the setup (of the water level), and the right-hand-side vector f contains the effects of the boundary conditions and the forces due to the surface waves. In the solver it is very efficient to calculate with direct addressing, so dry points are included in the vector x. This implies that the dimension of x and f are fixed and equal to $MXC \times MYC$. In the discretization a 9-point stencil is used. That implies that only 9 matrix elements per row are non-zero. These elements are stored in a diagonal-wise way. So for this part $NWKARR = 9$. The rows corresponding to dry points are filled with zeroes except on the main diagonal where the value 1 is substituted. The value of x and f are taken equal to 0 at these points.

Properties of the matrix

The discrete operator is symmetric in the inner region. This means that $a_{i,j} = a_{j,i}$. Due to the boundary conditions the symmetry of the operator is lost. The reasons for this are:

- When Dirichlet boundary conditions are used the known elements of x should be eliminated in order to keep the matrix symmetric. However this leads to a different dimension of A, x, and f, therefore the known elements are not eliminated.

- When dry points occur the derivation of the discrete boundary conditions is already complicated at the interface between wet and dry points. At this moment it is not clear how to discretize these conditions such that the resulting matrix is symmetric.

These difficulties motivate us to use a non-symmetric matrix. This is only a small drawback, because recently good methods have been developed to solve non-symmetric matrix vector systems.

When Neumann conditions are used on all boundaries the resulting matrix is singular. The solution is determined up to a constant. We have to keep this in mind during the construction of the solution procedure.

When Gauss elimination is used to solve equation (5.25), the zero elements in the bend of A become non-zero. This means that the required memory is equal to $2 \times MXC + 2$ vectors. For MXC large, this leads to an unacceptable large amount of memory. Therefore we use an iterative solution method, where the total amount of memory is less than the memory used in the discretization procedure.

The iterative solver

In 1D cases, the wave-induced set-up is calculated in SWAN with a simple trapezoidal rule.

In 2D cases, the Poisson equation of the divergence-free force field is solved in SWAN with a modified Successive Over Relaxation (SOR) technique (Botta and Ellenbroek, 1985). The boundary conditions for this elliptical partial differential equation are:

- at open boundaries: equilibrium between wave force and hydrostatic pressure gradient normal to the model boundary,
- at last grid points before shoreline: equilibrium between wave force and hydrostatic pressure gradient normal to the model boundary and
- at deepest boundary point: set-up is zero.

The shoreline in SWAN moves as dictated by the wave-induced set-up. The set-up computations are available in both the recti-linear and curvi-linear grids.

Chapter 6

Iterative solvers

This chapter is under preparation.

Chapter 7

Parallel implementation aspects

Domain decomposition methods have been successfully used for solving large sparse systems arising from finite difference or finite volume methods in computational fluid dynamics on distributed memory platforms. They are based, in essence, upon a partition of the whole computational domain in $\vec{x}$-space into a number of contiguous, non-overlapping subdomains with each of them being assigned to a different processor. In this case the same algorithm performs on all available processors and on its own set of data (known as the SPMD programming model). Each subdomain can have multiple neighbors on each of its four sides. For this, a data structure is implemented to store all the information about the relationship of the subdomain and its particular neighbors. Next, each subdomain, look in isolation, is then surrounded by an auxiliary layer of one to three grid points originating from neighbouring subdomains. This layer is used to store the so-called halo data from neighbouring subdomains that are needed for the solution within the subdomain in question. The choice of one, two or three grid points depends on the use of propagation scheme in geographical space, i.e., respectively, BSBT, SORDUP or Stelling/Leendertse. Since, each processor needs data that resides in other neighbouring subdomains, exchange of data across boundaries of subdomains is necessary. Moreover, to evaluate the stopping criterion (3.26), global communication is required. These message passings are implemented by a high level communication library such as MPI standard. A popular distribution is MPICH which is free software[1] and is used in the present study. Only simple point-to-point and collective communications have been

[1]Available from *http://www-unix.mcs.anl.gov/mpi/mpich*http://www-unix.mcs.anl.gov/mpi/mpich.

employed. There are, however, some other implementation and algorithmic issues that need to be addressed.

7.1 Load balancing

The mapping of subdomains on processors should be chosen so as to distribute the computational load as equally as possible and to minimize the communication cost. Intuitively, it will be clear that we have to allocate contiguous blocks of equal numbers of grid points on each processor. However, in the context of SWAN applications to coastal areas, some difficulties arise. Firstly, wet and dry grid points may unevenly distributed over subdomains while no computations have to be done in dry points. Secondly, an unbalanced partition may arise during the simulation due to the tidal effect (dry points become wet and vice versa). In such a case, one may decide to adapt the partition such that it is balanced again (so-called dynamic load balancing). Finally, most end-users are not willing to determine the partitioning themselves, thus automatic support for partitioning the grids is desirable.

In the present study, two well-established partition methods are applied. The first is called stripwise partitioning in which the computational grid is cut along one direction, resulting in horizontal or vertical strips. The choice of cutting direction depends on the interface size of the strips which should be minimized. However, the communication volume, which is related to the total size of the interfaces, can be further reduced by means of recursive application of alternately horizontal and vertical bisection. This is known as Recursive Co-ordinate Bisection (RCB). Further details on these techniques and an overview on grid partitioning can be found, e.g. in Fox (1988) and Chrisochoides *et al.* (1994). .

Within SWAN, the grid partitioning is carried out automatically on wet grid points only. The size of the subdomain equals the total number of wet points divided by the total number of subdomains. The implementation of a stripwise partitioning is as follows. First, an empty strip is created. Next, assign point-by-point to the created part until the size of that part has been reached. Thereafter, verify whether non-assigning wet points remain in the current strip. If so, these points will be assign to the same part too, otherwise create next empty strip. As a result, all strips have straight interfaces and include approximately the same number of wet grid points. Moreover, experiences with SWAN simulation have shown that the amount

of computations in each wet grid point remains more or less constant during the simulation and hence, there is no need for dynamic load balancing.

A final remark has to be made considering grid partitioning. The above described methodology does not seem to have been implemented in spectral wave models before. In Tolman (20020, another way of distributing data over the processors is discussed: each p^{th} wet grid point is assign to the same processor with p the total number of processors. The requirement of equal numbers of wet grid points per processor is provided automatically. However, it is impossible to compute the spatial wave propagation in an effective manner. The only alternative is to gather data for all grid points in a single processor before the calculation is performed. This will require a full data transpose, i.e. rearranging data distribution over separate processors. It is believed that this technique requires much more communication between processors than domain decomposition and therefore less suitable for SWAN.

7.2 Parallelization of implicit propagation schemes

Contrary to explicit schemes, implicit ones are more difficult to parallelize, because of the coupling introduced at subdomain interfaces. For example, concerning the four-sweep technique, during the first sweep, an update of $N(i, j, l, m)$ can be carried out as soon as $N(i-1, j, l, m)$ and $N(i, j-1, l, m)$ have been updated and thus it can not be performed in parallel. Parallelization of this implicit scheme requires modifications. Ideally, the parallel algorithm need no more computing operations than the sequential one for the same accuracy.

The simplest strategy to circumvent this problem consists in treating the data on subdomain interfaces explicitly, which in mathematical terms amounts to using a block Jacobi approximation of the implicit operator. In this context, we employ the RCB partition method, since it gives the required balanced, low-communication partitioning. This strategy possess a high degree of parallelism, but may lead to a certain degradation of convergence properties. However, this numerical overhead can be reduced by colouring the subdomains with four different colors and subsequently permuting the numbering of unknowns in four sweeps in accordance with the color of subdomains. Furthermore, each subdomain is surrounded by subblocks of different colors. See Figure 7.1. As a result, each coloured subdomain start with a different ordering of updates within the same sweep and thus reducing the

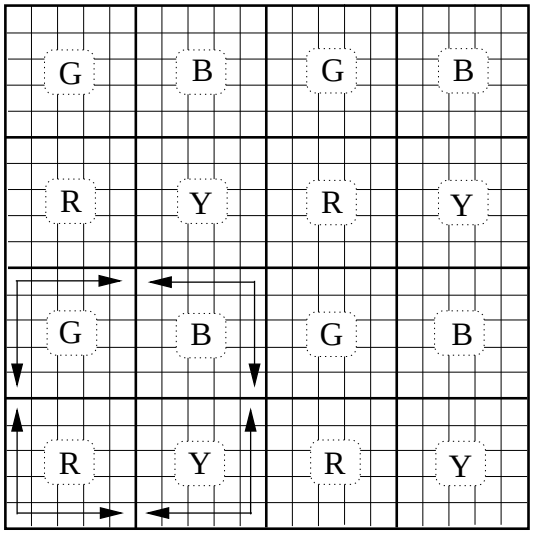

Figure 7.1: Four types of subblocks (red, yellow, green and black) treated differently with respect to the ordering of updates (indicated by arrows) per sweep.

number of synchronization points. This multicolor ordering technique has been proposed earlier, e.g. in Meurant (1988) and Van der Vorst (1989).

Another strategy is based on the ideas proposed by Bastian and Horton (1991) and is referred here to as the block wavefront approach. It is demonstrated with the following example. First, we decompose the computational domain into a number of strips. In this example, we assume that these strips are parallel to $y-$axis. Next, we start with the first sweep. The processor belonging to the first strip updates the unknowns $N(i, 1, l, m)$ along the first row $j = 1$. Thereafter, communication takes place between this processor and processor for strip 2. The unknowns $N(i, 2, l, m)$ along $j = 2$ in strip 1 and $N(i, 1, l, m)$ along $j = 1$ in strip 2 can be updated in parallel, and so on. After some start-up time all processors are busy. This is depicted in Figure 7.2. Finally, this process is repeated for the other three sweeps. Details can be found in the source code of SWAN 40.20. The block wavefront approach does not alter the order of computing operations of the sequential algorithm and thus preserving the convergence properties, but reduces parallel efficiency to a lesser extent because of the serial start-up and shutdown phases (Amdahl's law). This technique resembles much to the standard wavefront technique applied in a pointwise manner (unknowns on a diagonal

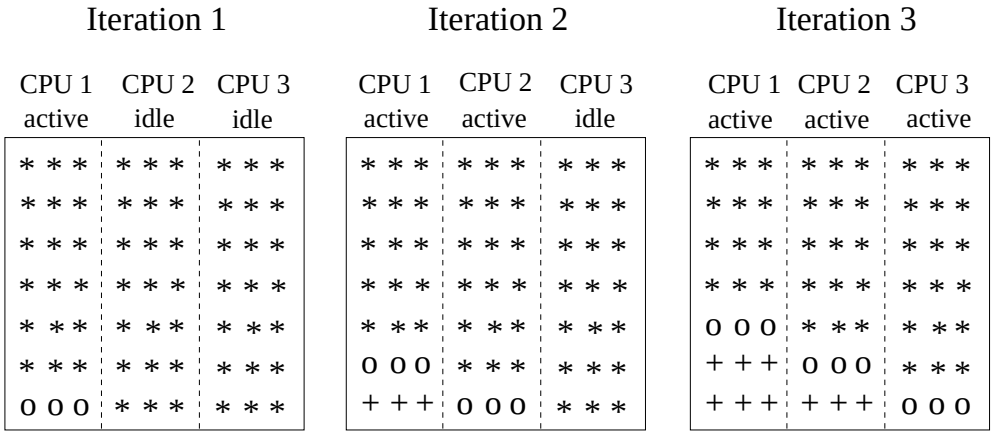

Figure 7.2: Application of block wavefront approach for the first 3 iterations during the first sweep. Domain is divided into 3 vertical strips. Stars represent unknowns to be updated, circles mean that unknowns are currently updated and the plus signs indicate unknowns that have been updated.

are mutually independent and thus can be updated in parallel; for details, see Templates (1994), which has also been employed by Campbell *et al.* (2002) for parallelizing SWAN using OpenMP.

The performance of the two discussed parallelization methods applied in the SWAN model has been discussed in (Zijlema, 2005). Numerical experiments have been run on a dedicated Beowulf cluster with a real-life application. They show that good speedups have been achieved with the block wavefront approach, as long as the computational domain is not divided into too thin slices. Moreover, it appears that this technique is sufficiently scalable. Concerning the block Jacobi method, a considerable decline in performance has been observed which is attributable to the numerical overhead arising from doubling the number of iterations. Furthermore, it may result in a solution that is computed to an accuracy that may not be realistic. In conclusion, parallelization with the block wavefront technique has been favoured and has been implemented in the current operational version of SWAN.

A survey of other alternatives to the parallelization of the implicit schemes is given in Templates (1994).

Chapter 8

The overall solution algorithm

Bibliography

[1] Abreu, M., A. Larraza and E. Thornton, 1992: Nonlinear transformation of directional wave spectra in shallow water, *J. Geophys. Res.*, **97**, 15579-15589

[2] Alves, J.H.G.M. and M.L. Banner, 2003: Performance of a saturation-based dissipation-rate source term in modelling the fetch-limited evolution of wind waves, *J. Phys. Oceanogr.*, **33**, 1274-1298

[3] Andorka Gal, J.H., L.H. Holthuijsen, J.C.M. de Jong and A.T.M.M. Kieftenburg, 1998: Wave transformation near a quasi-1D coast, *26th Int. Conf. Coastal Engng.*, Copenhagen, 150-160

[4] Arcilla, A.S. and C.M. Lemos, 1990: *Surf-Zone Hydrodynamics*, Centro Internacional de Métodos Numéricos en Ingenieria, Barcelona, 310 p.

[5] Arcilla, A.S., J.A. Roelvink, B.A. O'Connor, A.J.H.M. Reniers and J.A. Jimenez, 1994: The Delta flume '93 experiment, *Proc. Coastal Dynamics Conf. '94*, 488-502

[6] Banner, M.L. and I.R. Young, 1994: Modelling spectral dissipation in the evolution of wind waves. Part I: Assessment of existing model performance, *J. Phys. Oceanogr.*, **24**, No. 7, 1550-1571

[7] R. Barrett, M. Berry, T.F. Chan, J. Demmel, J. Donato, J. Dongarra, V. Eijkhout, R. Pozo, C. Romine, H. van der Vorst, Templates for the solution of linear systems: Building blocks for iterative methods, SIAM, Philadelphia, PA, 1994, accessible from *http://www.netlib.org/templates/Templates.html*http://www.netlib.org/templates/Templates.html

[8] P. Bastian, G. Horton, Parallelization of robust multi-grid methods: ILU factorization and frequency decomposition method, SIAM J. Sci. Stat. Comput. 12 (1991) 1457–1470.

[9] Battjes, J.A. and J.P.F.M. Janssen, 1978: Energy loss and set-up due to breaking of random waves, *Proc. 16*th *Int. Conf. Coastal Engineering*, ASCE, 569-587

[10] Battjes, J.A. and G.Ph. van Vledder, 1984, Verification of Kimura's theory for wave group statistics, *Proc. 19*th *Int. Conf. Coastal Engineering*, ASCE, Houston, 642-648

[11] Battjes, J.A. and M.J.F. Stive, 1985: Calibration and verification of a dissipation model for random breaking waves, *J. Geophys. Res.*, **90**, No. C5, 9159-9167

[12] Battjes, J.A. and S. Beji, 1992: Breaking waves propagating over a shoal, *Proc. 23*rd *Int. Conf. Coastal Engineering*, ASCE, 42-50

[13] Battjes, J.A., 1994: Shallow water wave modelling, M. Isaacson and M. Quick (Eds.), *Proc. Waves-Physical and Numerical Modelling*, University of British Columbia, Vancouver, 1-24

[14] Beji, S. and J.A. Battjes 1993: Experimental investigation of wave propagation over a bar, *Coastal Engineering*, **19**, 151-162

[15] Bender, L.C., 1996, Modification of the physics and numerics in a third-generation ocean wave model, *J. Atm. and Ocean. Techn.*, 13, 3, 726-750

[16] Bidlot, J.-R., B. Hansen and P.A.E.M. Janssen, 1996: Wave modelling and operational forecasting at ECMWF, *1*st *International Conference on EuroGOOS*, 7-11 October, 1996, The Hague, 206-213

[17] Benoit, M., F. Marcos and F. Becq, 1996: Development of a third-generation shallow-water wave model with unstructured spatial meshing. *Proc. 25*th *Int. Conf. Coastal Engineering*, ASCE, Orlando, 465-478

[18] Benoit, M., 2005: Evaluation of methods to compute the non-linear quadruplet interactions for deep-water wave spectra, *Proc. 5th Int. Symp. WAVES 2005*, Madrid, Spain

[19] Berkhoff, J.C.W., 1972: Computation of combined refraction-diffraction, *Proc. 13*th *Int. Conf. Coastal Engineering*, ASCE, 471-490

[20] Bertotti, L and L. Cavaleri, 1994: Accuracy of wind and wave evaluation in coastal regions, *Proc. 24*th *Int. Conf. Coastal Engineering*, ASCE, 57-67

[21] Booij, N., and L.H. Holthuijsen, 1987, Propagation of ocean waves in discrete spectral wave m*odels, Journal of Computational Physics*, vol. 68, 307-326.

[22] Booij, N., L.H. Holthuijsen and P.H.M. de Lange, 1992, The penetration of short-crested waves through a gap, *Proc. 23rd Int. Conf. Coastal Eng*, Venice 4-9 Oct., 1992, New York, 1993, 1044-1052

[23] Booij, N., L.H. Holthuijsen and R.C. Ris, 1996: The "SWAN" wave model for shallow water, *Proc. 25th Int. Conf. Coastal Engng.*, Orlando, 668-676

[24] Booij, N., L.H. Holthuijsen, N. Doorn and A.T.M.M. Kieftenburg, 1997: Diffraction in a spectral wave model, *Proc. 3rd Int. Symp. Ocean Wave Measurement and Analysis, WAVES'97*, ASCE, 234-255

[25] Booij, N., L.H. Holthuijsen and R. Padilla-Hernandez, 1997: A nonstationary, parametric coastal wave model, *Conf. Coastal Dynamics '97*, Plymouth, 99-107

[26] Booij, N., L.H. Holthuijsen and R. Padilla-Hernandez, 1997: Numerical wave propagation on a curvi-linear grid, *Proceedings 3rd International Symposium on Ocean Wave Measurement and Analysis, WAVES '97*, ASCE, 286-294

[27] Booij, N., L.H. Holthuijsen and R.C. Ris, 1998: Shallow water wave modelling, *Oceanology International 98, The Global Ocean, Brighton, Conference Proceedings*, 3, 483-491

[28] Booij, N., L.H. Holthuijsen and IJ.G. Haagsma, 1998: Comparing the second-generation HISWA wave model with the third-generation SWAN wave model, *5th International Workshop on Wave Hindcasting and Forecasting*, Melbourne, Florida, 215-222

[29] Booij, N., R.C. Ris and L.H. Holthuijsen, 1999, A third-generation wave model for coastal regions, Part I, Model description and validation, *J.Geoph.Research*, 104, C4, 7649-7666

[30] Booij, N., L.H. Holthuijsen and J.A. Battjes, 2001: Ocean to near-shore wave modelling with SWAN, *4th International Conference on Coastal Dynamics 2001*, Lund, Sweden, 335-344

[31] Booij, N., L.H. Holthuijsen and IJ.G. Haagsma, 2001: The effect of swell on the generation and dissipation of waves, *4th International Symposium on Ocean Wave Measurements and Analysis WAVES 2001*, San Francisco, 501-506

[32] Botta, E.F.F. and M.H.M. Ellenbroek, 1985: A modified SOR method for the Poisson equation in unsteady free-surface flow calculations, *J. Comput. Phys.*, **60**, 119-134

[33] Bouws, E. and J.A. Battjes, 1982: A Monte-Carlo approach to the computation of refraction of water waves, *J. Geophys. Res.*, **87**, 5718-5722

[34] Bouws, E. and G.J. Komen, 1983: On the balance between growth and dissipation in an extreme, depth-limited wind-sea in the southern North Sea, *J. Phys. Oceanogr.*, **13**, 1653−1658

[35] Campbell, T., J. Cazes, E. Rogers, Implementation of an important wave model on parallel architectures, in: Oceans 2002 MTS/IEEE Conference, IEEE, 2002, pp. 1509–1514, available from *http://www7320.nrlssc.navy.mil/mts2002/PDF/campbell-paper.pdf*http://www7320.nrlssc.navy.mil/mts2002/PDF/campbell-paper.pdf.

[36] Cardone, V.J., W.J. Pierson and E.G. Ward, 1976: Hindcasting the directional spectra of hurricane-generated waves, *J. Petr. Techn.*, **28**, 385-394

[37] Cavaleri, L. and P. Malanotte-Rizzoli, 1981: Wind wave prediction in shallow water: Theory and applications. *J. Geophys. Res.*, **86**, No. C11, 10,961-10,973

[38] Cavaleri, L. and L.H. Holthuijsen, 1998: Wave modelling in the WISE group, *Proc. 26th Int. Conf. Coastal Engng.*, Copenhagen, 498-508

[39] CERC, 1973: Shore Protection Manual, U.S. Army Corps of Engineers, Techn. Rep. No. 4, Vol. I

[40] Chen, Y. and H. Wang, 1983: Numerical model for nonstationary shallow water wave spectral transformations, *J. Geophys. Res.*, **88**, 9851-9863

[41] Chen, Y. and R.T. Guza, 1997: Modelling of breaking surface waves in shallow water, *J. Geophys. Res.*, 102, C11, 25035-25046

[42] Chrisochoides, N.P., E.N. Houstis, J.R. Rice, Mapping algorithms and software environment for data parallel PDE iterative solvers, J. Parallel and Distr. Comput. 21 (1994) 75–95.

[43] Collins, J.I., 1972: Prediction of shallow water spectra, *J. Geophys. Res.*, **77**, No. 15, 2693-2707

[44] Dingemans, M.W., A.C. Radder and H.J. de Vriend, 1978: Computations of the driving forces of wave-induced currents, *Coastal Engng.*, 11, 539-563

[45] De Waal, J.P., 2001. Wave growth limit in shallow water. Proc. 4th Int. Symp. Waves 2001, pp. 560–569.

[46] Dingemans, M.W., 1997: Water wave propagation over uneven bottoms. Part 1 -linear wave propagation, *Advanced Series on Ocean Engineering*, 13, World Scientific, 471 p.

[47] Eldeberky, Y., 1996: Nonlinear transformation of wave spectra in the nearshore zone, *Ph.D. thesis*, Delft University of Technology, Department of Civil Engineering, The Netherlands

[48] Eldeberky, Y. and J.A. Battjes, 1995: Parameterization of triad interactions in wave energy models, *Proc. Coastal Dynamics Conf. '95*, Gdansk, Poland, 140-148

[49] Eldeberky, Y. and J.A. Battjes, 1996: Spectral modelling of wave breaking: Application to Boussinesq equations, *J. Geophys. Res.*, **101**, No. C1, 1253-1264

[50] Elgar, S. and R.T. Guza, 1986: Nonlinear model predictions of bispectra of shoaling surface gravity waves, *J. Fluid Mech.*, 167, 1-18

[51] Elgar, S., R.T. Guza, B. Raubenheimer, T.H.C. Herbers and E.L. Gallagher, 1997: Spectral evolution of shoaling and breaking waves on a barred beach, *J. Geophys. Res.*, 102,C7, 15797-15805

[52] Ewing, J.A., 1971: A numerical wave prediction method for the North Atlantic Ocean, *Deutsch. Hydrogr. Z.*, **24**, No. 6, 241−261

[53] Ewing, J.A. and R.C. Hague, 1993: A second-generation wave model for coastal wave prediction, *Proc. of 2*nd *Int. Symposium on Ocean Wave Measurement and Analysis*, New Orleans, 576-589

[54] Fletcher, C.A.J., 1988: *Computational Techniques for Fluid Dynamics, Parts I and II,* Springer, 409+484 p.

[55] Ferziger, J.H. and Perić, M., 1999. Computational methods for fluid dynamics (2nd edition). Springer-Verlag, Berlin.

[56] G.C. Fox, A review of automatic load balancing and decomposition methods for the hypercube, in: M. Schulz (Ed.), Numerical Algorithms for Modern Parallel Computer Architectures, Springer, Verlag, 1988, pp. 63–76, IMA volume 13.

[57] Freilich, M.H. and R.T. Guza, 1984: nonlinear effects on shoaling surface gravity waves, *Phil. Trans. R. Soc. London,* A 311, 1-41

[58] Galvin, C.J., 1972: Wave breaking in shallow water, *Waves on beaches and resulting sediment transport*, Academic Press Inc., 413-455

[59] Gelci, R., H. Cazalé and J. Vassal, 1956: Utilization des diagrammes de propagation à la prévision énergétique de la houle, *Bulletin d'information du Comité Central d'océanographie et d'études des côtes*, **8**, No. 4, 160-197 (in French)

[60] Goda, Y, H. Takeda and Y. Moriya, 1967: Laboratory investigation of wave transmission over breakwaters*, Rep. port and Harbour Res. Inst.*, 13 (from Seelig, 1979)

[61] Golding, B.W., 1983: A wave prediction system for real-time sea state forecasting, *J. R. Met. Soc.*, **109**, 393-416

[62] Golub, G.H. and C.F. van Loan, 1986: Matrix Computations, North Oxford Academic, London, 476 p.

[63] Gorman, R.M. and C.G. Neilson, 1999: Modelling shallow water wave generation and transformation in an intertidal estuary, *Coastal Engineering*, 36, 197-217

[64] W. Gropp, E. Lusk, A. Skjellum, Using MPI: Portable parallel programming with the Messing Passing Interface, MIT Press, Cambridge, MA, 1999.

[65] Günther, H., S. Hasselmann and P.A.E.M. Janssen, 1992: The WAM model Cycle 4 (revised version), *Deutsch. Klim. Rechenzentrum, Techn. Rep. No. 4*, Hamburg, Germany

[66] Hargreaves, J.C. and Annan, J.D., 2001. Comments on "Improvement of the short-fetch behavior in the wave ocean model (WAM)". J. Atmos. Oceanic Techn., 18: 711–715.

[67] Hashimoto, N., H. Tsuruya and Y. Nakagawa, 1998: Numerical computations of the nonlinear energy transfer of gravity-wave spectra in finite water depths, *Coastal Engng. J.*, **40**, 23-40

[68] Hashimoto, N., IJ.G. Haagsma and L.H. Holthuijsen, 2002: Four-wave interactions in SWAN, *Proc. 28*$^{\text{th}}$ *Int. Conf. Coastal Engng.*, ASCE, Cardiff, 392-404

[69] Hasselmann, K., 1960: Grundgleichungen der Seegangsvoraussage, *Schiffstechnik*, 1, 191−195

[70] Hasselmann, K., 1962: On the non-linear transfer in a gravity wave spectrum, part 1. General theory, *J. Fluid Mech.*, **12**, 481-500

[71] Hasselmann, K., 1963a: On the non-linear transfer in a gravity wave spectrum, part 2. Conservation theory, wave-particle correspondence, irreversibility, *J. Fluid Mech.*, **15**, 273-281

[72] Hasselmann, K., 1963b: On the non-linear transfer in a gravity wave spectrum, part 3. Evaluation of energy flux and sea-swell interactions for a Neuman spectrum, *J. Fluid Mech.*, **15**, 385-398

[73] Hasselmann, K. and J.I. Collins, 1968: Spectral dissipation of finite-depth gravity waves due to turbulent bottom friction, *J. Mar. Res.*, **26**, 1-12

[74] Hasselmann, K., T.P. Barnett, E. Bouws, H. Carlson, D.E. Cartwright, K. Enke, J.A. Ewing, H. Gienapp, D.E. Hasselmann, P. Kruseman, A. Meerburg, P. Müller, D.J. Olbers, K. Richter, W. Sell and H. Walden, 1973: Measurements of wind−wave growth and swell decay during the Joint North Sea Wave Project (JONSWAP), *Dtsch. Hydrogr. Z.* Suppl., **12**, A8

[75] Hasselmann, K., 1974: On the spectral dissipation of ocean waves due to whitecapping, *Bound.-layer Meteor.*, **6**, 1-2, 107-127

[76] Hasselmann, K., D.B. Ross, P. Müller and W. Sell, 1976: A parametric wave prediction model, *J. Phys. Oceanogr.*, **6**, 200−228

[77] Hasselmann, S. and K. Hasselmann, 1981: A symmetrical method of computing the non-linear transfer in a gravity-wave spectrum, *Hamburger Geophys. Einzelschr.*, Serie A., 52, 8

[78] Hasselmann, S., K. Hasselmann, J.H. Allender and T.P. Barnett, 1985: Computations and parameterizations of the nonlinear energy transfer in a gravity wave spectrum. Part II: Parameterizations of the nonlinear transfer for application in wave models, *J. Phys. Oceanogr.*, **15**, 11, 1378-1391

[79] Hedges, T.S., 1987: Combination of waves and currents: an introduction, *Proc. Instn. Civ. Engrs.*, Part 1, **82**, 567-585

[80] Hersbach, H. and Janssen, P.A.E.M., 1999. Improvement of the short-fetch behavior in the wave ocean model (WAM). J. Atmos. Oceanic Techn., 16: 884–892.

[81] Herterich, K. and K. Hasselmann, 1980: A similarity relation for the nonlinear energy transfer in a finite-depth gravity-wave spectrum, *J. Fluid Mech.*, **97**, 215-224

[82] Holthuijsen, L.H., 1980: Methods of wave prediction, part I and II (Methoden voor golfvoorspelling, deel I en II, in Dutch), Technical Advisory Commission against Inundation (Technische Adviescommissie voor de Waterkeringen, in Dutch), Den Haag, The Netherlands

[83] Holthuijsen, L.H. and S. De Boer, 1988: Wave forecasting for moving and stationary targets, *Computer modelling in Ocean Engineering*, Eds.

B.Y. Schrefler and O.C. Zienkiewicz, Balkema, Rotterdam, The Netherlands, 231-234

[84] Holthuijsen, L.H., Booij, N. and T.H.C. Herbers, 1989: A prediction model for stationary, short-crested waves in shallow water with ambient currents, *Coastal Engineering*, **13**, 23-54

[85] Holthuijsen, L.H., N. Booij and R.C. Ris, 1993: A spectral wave model for the coastal zone, *Proceedings 2nd International Symposium on Ocean Wave Measurement and Analysis*, New Orleans, Louisiana, July 25−28, 1993: New York, pp. 630−641

[86] Holthuijsen, L.H., N. Booij and R. Padilla-Hernandez, 1997: A curvilinear, third-generation coastal wave model, *Conf. Coastal Dynamics '97*, Plymouth, 128-136

[87] Holthuijsen, L.H., N. Booij, R. Ris, J.H. Andorka Gal and J.C.M. de Jong, 1997: A verification of the third-generation wave model "SWAN" along the southern North Sea coast, *Proceedings 3rd International Symposium on Ocean Wave Measurement and Analysis, WAVES '97*, ASCE, 49-63

[88] Holthuijsen, L.H., 1998: The concept and features of the ocean wave spectrum, Provision and engineering/operational application of ocean wave spectra, *COST Conference*, UNESCO, 21-25 sept., Paris, keynote address, 11-20

[89] Holthuijsen, L.H., 1998: Waves in shallow water, *World Meteorological Organization Guide to wave analysis and forecasting*, WMO-N0. 702, Chapter 7, 81-88

[90] Holthuijsen, L.H., R.C. Ris and N. Booij, 1998: A verification of the third-generation wave model SWAN, *5th International Workshop on Wave Hindcasting and Forecasting*, Melbourne, Florida, 223-230

[91] Holthuijsen, L.H., N. Booij and IJ.G. Haagsma, 1998: Comparing 1st-, 2nd - and 3rd-generation coastal wave modelling, *26th Int. Conf. Coastal Engng.*, Copenhagen, 140-149

[92] Holthuijsen, L.H. and N. Booij, 2000: Oceanic and near-shore white-capping effects in SWAN, 6th Int. Workshop on Wave Hindcasting and Forecasting, Monterey, 362-368

[93] Holthuijsen, L.H, R.C. Ris, N. Booij and E.Cecchi, 2000: Swell and whitecapping, a numerical experiment, Proc. 27th Int. Conf. Coastal Engng., Sydney, 346-354

[94] Holthuijsen, L.H., Herman, A. and Booij, N., 2003: Phase-decoupled refraction-diffraction for spectral wave models, *Coastal Engineering*, **49**, 291-305

[95] Holthuijsen, L.H., 2005: *Waves in oceanic and coastal waters*, Cambridge University Press, in press.

[96] Hurdle, D.P. and G. Ph. van Vledder, 2004. *Proc. 23rd Int. Conf. on Offshore Mech. and Arctic. Eng.*

[97] Hsu, T.-W., S.-H. Ou and J.-M. Liau, 2005: Hindcasting nearshore wind waves using a FEM code for SWAN, *Coastal Engineering*, **52**, 177-195

[98] Janssen, P.A.E.M., 1989: Wave induced stress and the drag of air flow over sea waves, *J. Phys. Oceanogr.*, **19**, 745-754

[99] Janssen, P.A.E.M., 1991a: Quasi-linear theory of wind-wave generation applied to wave forecasting, *J. Phys. Oceanogr.*, **21**, 1631-1642

[100] Janssen, P.A.E.M., 1991b: Consequences of the effect of surface gravity waves on the mean air flow, *Int. Union of Theor. and Appl. Mech.* (IUTAM), Sydney, Australia, 193-198

[101] Jonsson, I.G. 1966: Wave boundary layers and friction factors, *Proc. 10th Int. Conf. Coastal Engineering*, ASCE, 127-148

[102] Jonsson, I.G., 1980: A new approach to rough turbulent boundary layers, *Ocean Engineering*, **7**, 109-152

[103] Jonsson, I.G., 1993: *The Sea*, Ocean Engineering Science, **9**, Part A

[104] Jonsson, I.G. and N.A. Carlsen, 1976: Experimental and theoretical investigations in an oscillatory turbulent boundary layer, *J. Hydraulic Research*, **14**, 45-60

[105] Kahma, K.K. and C.J. Calkoen, 1992: Reconciling discrepancies in the observed growth of wind−generated waves, *J. Phys. Oceanogr.*, **22**, 1389−1405

[106] Kaminsky, G.M. and N.C. Kraus, 1993: Evaluation of depth-limited wave breaking criteria, *Proc. of 2*nd *Int. Symposium on Ocean Wave Measurement and Analysis*, New Orleans, 180-193

[107] Karlson, T, 1969: Refraction of continuous ocean wave spectra, *Journal of Waterways, Ports, Harbours and Coastal Engineering*, ASCE, **95**, WW4, 275-287

[108] Kirby, J.T., 1986: Higher-order approximation in the parabolic equation method for water waves, *J. Geophys. Res.*, **91**, C1, 933-952

[109] Komen, G.J., S. Hasselmann, and K. Hasselmann, 1984: On the existence of a fully developed wind-sea spectrum, *J. Phys. Oceanogr.*, **14**, 1271-1285

[110] Komen, G.J., Cavaleri, L., Donelan, M., Hasselmann, K., Hasselmann, S. and P.A.E.M. Janssen, 1994: *Dynamics and Modelling of Ocean Waves*, Cambridge University Press, 532 p.

[111] Kuik, A.J., G.Ph. van Vledder and L.H. Holthuijsen, 1988: A method for the routine analysis of pitch-and-roll buoy wave data, *J. Phys. Oceanogr.*, **18**, 1020-1034

[112] Li, C.W. and M. Mao, 1992: Spectral modelling of typhoon-generated waves in shallow waters, *J. Hydraulic Research*, **30**, 5, 611-622

[113] Lin, R.Q. and N.E. Huang, 1996: the Goddard coastal wave model. Part I: Numerical method, *J. Phys. Oceanogr.*, **26**, 833-847

[114] Liu, P.L., S.B. Yoon and J.T. Kirby, 1985: Nonlinear refraction-diffraction of waves in shallow water, *J. Fluid Mech.*, 153, 185-201

[115] Luo, W. and J. Monbaliu, 1994: Effects of the bottom friction formulation on the energy balance for gravity waves in shallow water, *J. Geophys. Res.*, **99**, C9, 18,501-18,511

[116] Madsen, O.S., Y.-K. Poon and H.C. Graber, 1988: Spectral wave attenuation by bottom friction: Theory, *Proc. 21*th *Int. Conf. Coastal Engineering*, ASCE, 492-504

[117] Madsen, P.A. and O.R. Sørensen, 1992: A new form of the Boussinesq equations with improved linear dispersion characteristics. Part 2: A slowly-varying bathymetry, *Coastal Engineering*, **18**, 183-205

[118] Madsen, P.A. and O.R. Sørensen, 1993: Bound waves and triad interactions in shallow water, *Ocean Engineering,* **20**, 4, 359-388

[119] Mase, H. and J.T. Kirby, 1992: Hybrid frequency-domain KdV equation for random wave transformation, *Proc. 23*th *Int. Conf. Coastal Engineering*, ASCE, 474-487

[120] Mastenbroek, C., G. Burgers, and P.A.E.M. Janssen, 1993: The dynamical coupling of a wave model in a storm surge model through the atmospheric boundary layer, *J. Phys. Oceanogr.*, **23**, 1856-1866

[121] Mei, C.C., 1983: *The applied dynamics of ocean surface waves*, Wiley, New York, 740 p.

[122] G. Meurant, Domain decomposition methods for partial-differential equations on parallel computers, Int. J. Supercomputer Appl. and High Perform. Comput. 2 (4) (1988) 5–12.

[123] Miles, J.W., 1957: On the generation of surface waves by shear flows, *J. Fluid Mech.*, **3**, 185−204

[124] Miles, J.W., 1981: Hamiltonian formulations for surface waves, *Applied Scientific Research*, **37**, 103-110

[125] Nelson, R.C., 1987: Design wave heights on very mild slopes: An experimental study, *Civil. Eng. Trans., Inst. Eng. Aust.*, **29**, 157-161

[126] Nelson, R.C., 1994: Depth limited wave heights in very flat regions, *Coastal Engineering*, **23**, 43-59

[127] Nelson, R.C., 1997: Height limits in top down and bottom up wave environments, *Coastal Engineering*, **32**, 247-254

[128] Nwogu, O., 1994: Nonlinear evolution of directional wave spectra in shallow water, *Proc. 24*th *Int. Conf. Coastal Engineering*, ASCE, 467-481

[129] OpenMP ARB, OpenMP, *http://www.openmp.org*http://www.openmp.org.

[130] Padilla-Hernandez, R., P. Osuna, J. Monbaliu and L. Holthuijsen, 1998: Intercomparing third-generation wave model nesting, *5th International Workshop on Wave Hindcasting and Forecasting*, Melbourne, Florida, 102-112

[131] Peregrine, D.H., 1966: Long waves on a beach, *J. Fluid Mech.*, **27**, 4, 815-827

[132] Phillips, O.M., 1957: On the generation of waves by turbulent wind, *J. Fluid Mech.*, **2**, 417−445

[133] Phillips, O.M., 1960: On the dynamics of unsteady gravity waves of finite amplitude. Part 1, *J. Fluid Mech.*, **9**, 193-217

[134] Phillips, O.M., 1977: *The dynamics of the upper ocean*, Cambridge University Press, 336 p.

[135] Phillips, O.M., 1985: Spectral and statistical properties of the equilibrium range in wind-generated gravity waves, *J. Fluid Mech.*, **156**, 505-531

[136] Pierson, W.J. and L. Moskowitz, 1964: A proposed spectral form for fully developed wind seas based on the similarity theory of S.A. Kitaigorodskii, *J. Geophys. Res.*, **69**, 24, 5181-5190

[137] Piest, J., 1965: Seegangsbestimmung und Seegangsrefraktion in einem Meer mit nicht- ebenem Boden; eine theoretische Untersuchung, *Deutsch. Hydrogr. Z.*, **18**: 67-74 (in German)

[138] Press, W.H., Flannery, B.P., Teukolsky, S.A. and Vetterling, W.T., 1993. Numerical recipes in Fortran 77. The art of scientific computing (2nd edition). Cambridge University Press, New York (available from *http://www.nr.com*http://www.nr.com).

[139] Putnam, J.A. and J.W. Johnson, 1949: The dissipation of wave energy by bottom friction, *Trans. Am. Geoph. Union*, **30**, 67-74

[140] Radder, A.C., 1979: On the parabolic equation method for water-wave propagation, *J. Fluid Mech.*, **95**, 159-176

[141] Radder, A.C., 1992: An explicit Hamiltonian formulation of surface waves in water of finite depth, *J. Fluid Mech.*, **237**, 435-455

[142] Radder, A.C., 1996: Hamiltonian dynamics of water waves, *Advances of Coastal and Ocean Engineering*, World Scientific, **4**, ??-??

[143] Resio, D. and W. Perrie, 1991: A numerical study of nonlinear energy fluxes due to wave-wave interactions. Part I: Methodology and basic results, *J. Fluid Mech.*, **223**, 609-629

[144] Resio, D.T., J.H. Pihl, B.A. Tracy and C.L. Vincent, 2001: Nonlinear energy fluxes and the finite depth equilibrium range wave spectra, *J. Geophys. Res.*, **106**, C4, 6985-7000.

[145] Resio, D.T., C.E. Long and C.L. Vincent, 2004: Equilibrium-range constant in wind-generated wave spectra, *J. Geophys. Res.*, **109**, C01018.

[146] Ris, R.C., L.H. Holthuijsen and N. Booij, 1994: A spectral model for waves in the near shore zone, *Proc. 24th Int. Conf. Coastal Engng*, Kobe, Japan, pp. 68-78

[147] Ris, R.C. and L.H. Holthuijsen, 1997: Modelling of current induced wave-blocking in a spectral wave model, *8*$^{\text{th}}$ *International Biennal Conference on Physics of Estuaries and Coastal Seas*, J. Dronkers and M.B.A.M. Scheffers (eds.), The Hague, 139-144

[148] Ris, R.C., 1999. Model convergence of SWAN in the Westerschelde estuary. WL|Delft Hydraulics, Report H3496.

[149] Ris, R.C., N. Booij and L.H. Holthuijsen, 1999: A third-generation wave model for coastal regions, Part II: Verification, *J. Geophys. Res.*, 104, C4, 7667-7681

[150] Ris, R., L.H. Holthuijsen, J.M. Smith, N. Booij and A.R. van Dongeren, 2002: The ONR virtual testbed for coastal and oceanic wave models, *Proc. 28*$^{\text{th}}$ *Int. Conf. Coastal Engng.*, ASCE, Cardiff, 380-391

[151] Roache, P.J., 1972: *Computational Fluid Dynamics*, Hermosa Publishers, Albuquerque, 446 p.

[152] Rogers, W.E., J.M. Kaihatu, H.A. H. Petit, N. Booij, and L.H. Holthuijsen, 2002: Diffusion reduction in a arbitrary scale third generation wind wave model, *Ocean Engng.*, **29**, 1357-1390.

[153] Rogers, W.E., P.A. Hwang and D.W. Wang, 2003: Investigation of wave growth and decay in the SWAN model: three regional-scale applications, *J. Phys. Oceanogr.*, **33**, 366-389.

[154] Sakai, T., M. Koseki and Y. Iwagaki, 1983: Irregular wave refraction due to current, *J. of Hydr. Eng.*, ASCE, **109**, 9, 1203-1215

[155] Sanders, J.W., 1976: A growth-stage scaling model for the wind-driven sea, *Deutsch. Hydrogr. Z.*, **29**, 136-161

[156] Seelig, W.N., 1979, Effects of breakwaters on waves: laboratory tests of wave transmission by overtopping, *Proc. Conf. Coastal Structures*, 79, 2, 941-961

[157] Shemdin, P., K. Hasselmann, S.V. Hsiao and K. Herterich, 1978: Non−linear and linear bottom interaction effects in shallow water, in: Turbulent Fluxes through the Sea Surface, *Wave Dynamics and Prediction, NATO Conf. Ser.*, **V**, 1, 347−372

[158] Snyder, R.L., Dobson, F.W., Elliott, J.A. and R.B. Long, 1981: Array measurement of atmospheric pressure fluctuations above surface gravity waves, *J. Fluid Mech.*, **102**, 1-59

[159] Stelling, G.S. and J.J. Leendertse, 1992: Approximation of convective processes by cyclic AOI methods, *Proceeding 2nd international conference on estuarine and coastal modeling*, ASCE Tampa, Florida, 771-782

[160] Stone, H.L., 1968: Iterative solution of implicit approximations of multidimensional partial differential equations, *SIAM J. of Numer. Anal.*, **5**, 530−558

[161] SWAMP group, 1985: *Ocean wave modelling*, Plenum Press, New York and London

[162] Taylor, P.A. and R.J. Lee, 1984: Simple guidelines for estimating wind speed variations due to small-scale topographic features, *Climatol. Bull.*, 18, 3-32

[163] Thornton, E.B. and R.T. Guza, 1983: Transformation of wave height distribution, *J. Geophys. Res.*, **88**, C10, 5925-5938

[164] Tolman, H.L., 1990: Wind wave propagation in tidal seas, *Ph.D. thesis*, Delft University of Technology, Department of Civil Engineering, The Netherlands

[165] Tolman, H.L., 1991: A third-generation model for wind waves on slowly varying, unsteady and inhomogeneous depths and currents, *J. Phys. Oceanogr.*, **21**, 6, 782-797

[166] Tolman, H.J., 1992a: Effects of numerics on the physics in a third-generation wind-wave model, *J. Phys. Oceanogr.*, **22**, 10, 1095-1111

[167] Tolman, H.L., 1992b: An evaluation of expressions for the wave energy dissipation due to bottom friction in the presence of currents, *Coastal Engineering*, **16**, 165-179

[168] Tolman, H. L., 1995: On the selection of propagation schemes for a spectral wind−wave model. *NWS/NCEP Office Note 411*, 30 pp. + figures.

[169] Tolman, H.L., 2002: Distributed-memory concepts in the wave model WAVEWATCH III, *Parallel Comput.*, **28**, 35-52.

[170] Tracy, B. and D.T. Resio, 1982: Theory and calculation of the nonlinear energy transfer between sea waves in deep water. WES Report 11, US Army Corps of Engineers.

[171] Van Vledder, G. Ph., J.G. de Ronde and M.J.F. Stive, 1994: Performance of a spectral wind-wave model in shallow water, *Proc. 24*$^{\text{th}}$ *Int. Conf. Coastal Engineering*, ASCE, 761-774

[172] Van Vledder, G. Ph. and D.P. Hurdle, 2002: Performance of formulations for whitecapping in wave prediction models, *Proc. OMAE 2002*

[173] Van Vledder, G. Ph. and M. Bottema, 2003: Improved modelling of nonlinear four-wave interactions in shallow water, *Proc. 28*$^{\text{th}}$ *Int. Conf. Coastal Engineering*, ASCE, 459-471

[174] Van Vledder, G. Ph., 2006: The WRT method for the computation of non-linear four-wave interactions in discrete spectral wave models, *Coast. Engng.*, **53**, 223-242

[175] Vincent, C.L., J.M. Smith and J. Davis, 1994: Parameterization of wave breaking in models, *Proc. of Int. Symp.: Waves - Physical and Numerical Modelling*, Univ. of British Columbia, Vancouver, Canada, M. Isaacson and M. Quick (Eds.), Vol. II, 753-762

[176] H.A. van der Vorst, High performance preconditioning, SIAM J. Sci. Stat. Comput. 10 (1989) 1174–1185.

[177] WAMDI group, 1988: The WAM model − a third generation ocean wave prediction model, *J. Phys. Oceanogr.*, **18**, 1775−1810

[178] Webb, D.J., 1978: Non-linear transfers between sea waves, *Deep-Sea Res.*, **25**, 279-298

[179] Weber, S.L., 1989: Surface gravity waves and turbulent bottom friction, *Ph.D. thesis*, University of Utrecht, The Netherlands

[180] Weber, S.L., 1991a: Bottom friction for wind sea and swell in extreme depth-limited situations, *J. Phys. Oceanogr.*, **21**, 149-172

[181] Weber, S.L., 1991b: Eddy-viscosity and drag-law models for random ocean wave dissipation, *J. Fluid Mech.*, **232**, 73-98

[182] P. Wesseling, An introduction to multigrid methods, John Wiley and Sons, Chichester, 1992.

[183] Van der Westhuysen, A.J., M. Zijlema and J.A. Battjes, 2006: Nonlinear saturation-based whitecapping dissipation in SWAN for deep and shallow water, to appear in *Coast. Engng.*

[184] Wilson, B.W., 1965: Numerical prediction of ocean waves in the North Atlantic for December 1959, *Deutsch. Hydrogr. Z.*, **18**, 3, p. 114-130

[185] Whitham, G.B., 1974: *Linear and nonlinear waves*, Wiley, New York, 636 p.

[186] Wu, J., 1982: Wind-stress coefficients over sea surface from breeze to hurricane, *J. Geophys. Res.*, **87**, C12, 9704-9706

[187] Yan, L. 1987: An improved wind input source term for third generation ocean wave modelling, *Scientific report* WR-No 87-8, De Bilt, The Netherlands

[188] Yamaguchi, M., 1986: A numerical model of nearshore currents based on a finite amplitude wave theory, *Proc. 20*th *Int. Conf. Coastal Engineering*, ASCE, 849-863

[189] Yamaguchi, M., 1988: A numerical model of nearshore currents due to irregular waves, *Proc. 21*th *Int. Conf. Coastal Engineering*, ASCE, 1113-1126

[190] Yamaguchi, M., 1990: A numerical model for refraction computation of irregular waves due to time-varying currents and water depth, *Proc. 22*th *Int. Conf. Coastal Engineering*, ASCE, 205-217

[191] Young, I.R., 1988: A shallow water spectral wave model, *J. Geophys. Res.*, **93**, C5, 5113-5129

[192] Young, I.R., 1999: Wind generated ocean waves, Eds. R. Bhattacharyya and M.E. McCormick, Ocean Engineering Series, Elsevier, Amsterdam, 288 p.

[193] Young, I.R., and M.L. Banner, 1992: Numerical Experiments on the evolution of fetch limited waves, *Int. Union of Theor. and Appl. Mech. (IUTAM)*, Sydney, Australia, 267-275

[194] Young, I.R. and G. Ph. van Vledder, 1993: A review of the central role of nonlinear interactions in wind-wave evolution, *Phil. trans. R. Soc. London.* A., **342**, 505-524

[195] Young, I.R. and L.A. Verhagen, 1996a: The growth of fetch limited waves in water of finite depth. Part 1: Total energy and peak frequency, *Coastal Engineering*, **29**, 47-78

[196] Young, I.R. and L.A. Verhagen, 1996b: The growth of fetch limited waves in water of finite depth. Part 2: Spectral evolution, *Coastal Engineering*, **29**, 79-99

[197] Young, I.R. and L.A. Verhagen, 1996c: The growth of fetch limited waves in water of finite depth. Part 3: Directional spectra, *Coastal Engineering*, **29**, 101-121

[198] Zijlema, M. and Wesseling, P., 1998. Higher-order flux-limiting schemes for the finite volume computation of incompressible flow. Int. J. Comput. Fluid Dyn., 9:89–109.

[199] Zijlema, M., 2005: Parallelization of a nearshore wind wave model for distributed memory architectures, in *Parallel Computational Fluid Dynamics - Multidisciplinary applications*, Eds. G. Winter and A. Ecer and J. Periaux and N. Satofuka and P. Fox, Elsevier Science B.V., Amsterdam, The Netherlands, 207-214

[200] Zijlema, M. and A.J. van der Westhuysen: On convergence behaviour and numerical accuracy in stationary SWAN simulation of nearshore wind wave spectra. *Coastal Engineering*, **52**, 237-256.

Index